



HHS Public Access

Author manuscript

Lab Invest. Author manuscript; available in PMC 2015 October 01.

Published in final edited form as:

Lab Invest. 2015 April ; 95(4): 432–452. doi:10.1038/labinvest.2014.154.

Application of GFP imaging in cancer

Robert M. Hoffman

AntiCancer, Inc., Dept. of Surgery, University of California San Diego

Abstract

Multicolored proteins have allowed the color coding of cancer cells growing *in vivo* and enabled the distinction of host from tumor with single-cell resolution. Non-invasive imaging with fluorescent proteins enabled follow the dynamics of metastatic cancer to be followed in real time in individual animals. Non-invasive imaging of cancer cells expressing fluorescent proteins has enabled the real-time determination of efficacy of candidate antitumor and antimetastatic agents in mouse models. The use of fluorescent proteins to differentially label cancer cells in the nucleus and cytoplasm allow visualization of the nuclear–cytoplasmic dynamics of cancer cells *in vivo*, mitosis, apoptosis, cell-cycle position and differential behavior of nucleus and cytoplasm such as occurs during cancer-cell deformation and extravasation. Recent applications of the technology described here include linking fluorescent proteins with cell-cycle-specific proteins (FUCCI) such that the cells change color from red to green as they transit from G1 to S phases. With the macro and micro imaging technologies described here, essentially any *in vivo* process can be imaged, enabling the new field of *in vivo* cell biology using fluorescent proteins.

Keywords

GFP; RFP; CFP; imaging; color-coded; non-invasive; intravital; confocal; nude mice; orthotopic; tumor; metastasis; cell trafficking; mitosis; apoptosis; cell cycle; drug treatment

Introduction

When the Nobel Prize in chemistry was awarded for the discovery of green fluorescent protein (GFP) in 2008, the Nobel Committee called GFP a guiding star for biochemistry enabling processes that were previously invisible, such as cancer cells spreading, to be strikingly visible. GFP and its red, blue, yellow, and orange cousins have revolutionized biomedical research and enabled every major disease, both cause and effect, to “light-up” in the laboratory for researchers to visualize, understand and eventually conquer them. Fluorescent proteins allow us to visualize, in real time, all important aspects of cancer in living animals, including cancer cell cycle, mitosis, apoptosis, motility, invasion, metastasis and

Users may view, print, copy, and download text and data-mine the content in such documents, for the purposes of academic research, subject always to the full Conditions of use:http://www.nature.com/authors/editorial_policies/license.html#terms

Correspondence to: Robert M. Hoffman, Ph.D., 7917 Ostrow Street, San Diego, CA 92111 USA, Tel: 858-654-2555, Fax: 858-268-4175, all@anticancer.com.

Dedication: This article is dedicated to the memory of A.R. Moossa, M.D.

Conflict of Interest: Robert M. Hoffman is an unsalaried affiliate of AntiCancer Inc.

angiogenesis. Multicolored proteins have allowed the color-coding of cancer cells growing *in vivo* and enabled the distinction of host from tumor with single-cell resolution.¹

Fluorescent proteins of many different colors have now been characterized and these can be used to color-code cancer cells of a specific genotype or phenotype. For example, the behavior of cancer stem cells labeled with green fluorescent protein (GFP) and non-stem cells labeled with red fluorescent protein (RFP) can be simultaneously compared *in vivo*. The stroma and the cancer cells can be color-coded with fluorescent proteins. For example, a transgenic mouse expressing GFP in all of its cells (or in specific cells such as endothelial cells) transplanted with cancer cells expressing RFP enables the interaction between the cancer cells and the host cells to be visualized in real time.

The long wavelength excitation of some fluorescent proteins, such as Katushka,² also reduces the extent of photobleaching and enables deep imaging. Therefore, real-time imaging of tumor growth and metastasis can be carried out in the intact animal in deep tissues. For singlecell resolution, reversible skin-flaps as well as chronic-transparent window models can be used over many parts of the body (skin, brain, lung, liver, etc.).³⁻⁵ Real-time imaging with fluorescent proteins is especially important when evaluating the efficacy of therapeutics on metastasis, tumor recurrence⁶ and cell cycle dependence.

Properties of GFP and other fluorescent proteins as imaging agents

GFP and related fluorescent proteins are a family of proteins with emission spectra ranging from 442 to over 650 nm.⁷ There are many spectrally distinct fluorescent proteins resulting in a palette of colors⁸ that can be simultaneously imaged. Fluorescent proteins range in size from 25 to 30 kDa and form internal chromophores that do not require cofactors or substrates to fluoresce. Fluorescent proteins generally have very high extinction coefficients ranging up to approximately $\epsilon = 95,000$. In addition, fluorescent proteins have very high quantum yields up to 0.8.⁹ These properties make fluorescent proteins very bright. Two-photon absorption of GFP is important for deep tissue imaging *in vivo*. Another important feature of fluorescent protein is the spectral distinction between many members of the family, enabling a palette of multicolor fluorescent proteins that can be used simultaneously for multifunctional *in vivo* imaging. Spectral separation imaging is also very useful to distinguish different colors including autofluorescence.

In vivo imaging with fluorescent proteins

Fluorescent proteins are so bright that simple equipment can be used for *in vivo* imaging. Macroimaging studies requires equipment as simple as an LED flashlight with appropriate excitation filters and another emission filters.¹⁰ *In vivo* images can even be acquired with a cell phone camera!

A fluorescence light box with fiber-optic lighting at approximately 490 nm and appropriate filters, placed on top of the light box, can be used to image tumors and metastasis that can be viewed with a camera with an appropriate filter to enable the images to be displayed on a monitor and digitally stored.¹¹ Excitation with a narrow band filter at approximately 490 nm should be used. Fluorescence emission can be observed through a 520 nm long-pass filter.¹¹

A powerful hand-held imaging device can be used that inputs the image directly to a computer monitor can also be used.¹²

A variable-magnification small animals imaging system (OV100, Olympus Corp., Tokyo, Japan), containing an MT-20 light source (Olympus Biosystems, Planegg, Germany) and DP70 CCD camera (Olympus), can be used for macro and subcellular imaging in live mice. The optics of the OV100 fluorescence imaging system have been specially developed for macroimaging as well as microimaging with high light-gathering capacity. The objectives have high numerical aperture and are long working distance. Individually optimized objective lenses, parcentered and parfocal, provide a 105-fold magnification range for imaging of the entire body down to the subcellular level without disturbing the animal. The OV100 has the lenses mounted on an automated turret with a high magnification range of $\times 1.6$ to $\times 16$ and a field of view ranging from 6.9 to 0.69 mm. The optics and anti-reflective coatings ensure optimal imaging of multiplexed fluorescent reporters in small animals (Figure 1).¹³

The use of tunable filters allows the isolation of any individual spectrum in any fluorescent pixel. This technique eliminates autofluorescence as well as enabling high-resolution spectral distinction when multiple fluorescent proteins are being used. Spectral resolution enables imaging of tumor on deep tissues or high-resolution non-invasive visualization of tumor blood vessels¹⁴ which expresses a fluorescent protein of a different color than the two.

Ex vivo imaging using fluorescent proteins

The first use of GFP for *in vivo* imaging, visualized cancer cells growing in athymic nude mice in our laboratory.¹⁵ Cancer cells were stably transfected with GFP and were transplanted into several mouse models, including orthotopic models that have a high metastatic capacity. Metastases could be observed in any organ at the single-cell level in unprocessed tissues. In addition, cells were visualized in the process of intravasation and extravasation. The visualization of single cancer cells in tissue is beyond the capabilities of standard histological techniques.

Intravital imaging using fluorescent proteins

Previous to our laboratory's pioneering use of GFP for *in vivo* imaging, *in vivo* fluorescence imaging was limited to the visualization of cells that were transiently labeled with vital dyes. Use of fluorescent proteins, now allows the direct imaging of single cells *in vivo* for unlimited periods.

Reversible skin-flaps can also be introduced onto different parts of the animal to image single cancer cells or small colonies on internal organs.³ The skin-flaps are reversed by simple suturing. External imaging can then be done through the relatively transparent body walls of the mouse, which include the skull at the single cell level, by use of a simple fluorescence dissecting microscope or more sophisticated equipment described below. Blood vessels growing on tumors can also be observed using skin flaps because they contrast with the fluorescence of the tumors.³

With intravital microscopy,¹⁶ imaging through the opened skin or body walls of live mice single cancer cells have been visualized. All steps in the metastatic process can be visualized. Individual, nondividing cells as well as micro- and macrometastases can be clearly visualized and quantified. Cellular details, such as pseudopodial projections, can be clearly seen.¹⁷ In early studies, Farina et al.¹⁸ observed cancer cell invasion at the single-cell level, including intravasation and extravasation, using GFP-expressing cells. Condeelis et al.¹⁹ used confocal GFP imaging to observe the polarity of cancer cells responding to chemotactic cytokines by intravital imaging.

Multiphoton laser-scanning microscopy

Multiphoton laser-scanning microscopy (MPLSM)²⁰ can provide high-resolution to image deeper regions of GFP-expressing tumors.^{17,18} Fukumura et al.^{21,22} monitored the activity of the vascular endothelial growth factor (VEGF) promoter in transgenic mice that expressed GFP under the control of the VEGF promoter. MPLSM showed that the tumor was able to induce activity of the VEGF promoter and subsequent blood-vessel formation.^{21,22}

Color-coded imaging of tumor angiogenesis

Following transplantation of the RFP-expressing murine melanoma cell line B16F10 into transgenic mice in which the promoter of the gene coding for the stem cell-marker nestin drives GFP (ND-GFP). Angiogenesis was visualized using dual-color fluorescence imaging, since NDGFP was expressed in the proliferating endothelial cells and nascent blood vessels in the growing tumor which was labeled with RFP. Color-coded imaging demonstrates that doxorubicin inhibited tumor angiogenesis as well as tumor growth in these mice.²³

The stem cells are endothelial cell precursors. For state-of-the-art information on nestin-GFP expression, please see Matsuzaki et al.²⁴

Imaging GFP-labeled cancer cells in blood vessels

Cancer cell trafficking in blood vessels was originally observed in real time after injection of GFP-expressing cancer cells in the tail vein of mice.²⁵ Lung carcinoma cells²⁶ and mammary cancer cells,²⁷ both expressing GFP, interacted with the blood-vessel wall as seen via skin window chambers in rodents. Angiogenesis was induced by as few as 60-80 cancer cells. In the surrounding tissue, increased vasodilation and changes in blood-vessel morphology were also observed. Angiogenesis was also visualized using a GFP-expressing gliosarcoma rodent cell line.²⁸

Hematogenous metastases containing GFP cancer cells were visualized in intact perfused mouse and rat lung. The GFP-expressing cells were visualized attached to the endothelia of pulmonary precapillary arterioles and capillaries as well as in colonies formed within the blood vessels.^{29,30}

PC-3-GFP human prostate cancer cells metastasized from the orthotopic site to within the blood vessels of the liver and the lung, where they proliferated. The intravascular cancer

cells produced their own microenvironment, where they could continue to proliferate. Extravasation occurred earlier in the lung than in the liver.³¹

HT-1080 human fibrosarcoma cells, labeled with a red fluorescent protein (mCherry), linked to histone H2B, was expressed in the nucleus and FP was expressed in the cytoplasm. Cancer cells were injected in the epigastric cranialis vein in an abdominal flap of nude mice as an imaging model. The cell cycle position of individual living cells was visualized by the nuclear-cytoplasmic ratio and nuclear morphology. Real-time induction of apoptosis was observed by nuclear size changes and progressive nuclear fragmentation. Intra- and extravascular mitotic cells were also visualized. One hour after cell injection, round and elongated cancer cells were observed in the vessels. Five hours after injection, dual-color cancer cells began to divide within the vessel. By 10 h, some intravascular cancer cells underwent apoptosis. Deformed new blood vessels in the tumor were observed 10 days later. Extravascular cancer cells were imaged dividing in the tumor at day 14 after injection.³²

In order to study cytoplasmic and nuclear deformation, dual-color cancer cells expressing GFP in the nucleus and RFP in the cytoplasm were injected intracardially. Cancer cells which reached capillaries in the capillaries elongated to fit the width of these vessels. The average length of the major axis of the cancer cells in the capillaries increased to 3.97 times their normal length and nuclei increased their length 1.64 times in the capillaries. Non-dividing cancer cells in capillaries over 8 μm in diameter could migrate up to $48.3 \mu\text{m hr}^{-1}$.³³ The limits of cell migration may depend on deformation of the nucleus, as shown with the dual-color cancer cells expressing GFP in the nucleus and RFP in the cytoplasm.³⁴

The nuclear and cytoplasmic behavior of dual color cancer cells with GFP in the nucleus and RFP in the cytoplasm were imaged in real time in large blood vessels as they moved by various means or adhered to the vessel surface in the abdominal skin flap. During extravasation, real-time dual-color imaging showed that cytoplasmic processes of the cancer cells exited the vessels first, with nuclei following along the cytoplasmic projections. Both cytoplasm and nuclei underwent deformation during extravasation.¹³

GFP-expressing metastatic (MTLn3) and non-metastatic (MTC) cell lines (derived from the rat mammary adenocarcinoma 13762 NF cell line) were compared for their behavior in blood vessels. The metastatic cells had a greater affinity for blood vessels. In contrast, whereas the non-metastatic cells lost part of their cytoplasm when interacting with the vessel wall, possibly as a result of the shearing of cell pseudopods that are inserted into the blood flow during intravasation.¹⁹

Cancer cell trafficking in lymphatic channels imaged with RFP and RFP

GFP/RFP labeled cancer cells trafficked through lymphatic vessels where they were imaged via a skin flap in real time at the cellular level until they entered the axillary lymph node.³⁵

Transdifferentiation of cancer cells into blood vessel cells

GFP-labeled colon carcinoma were also visualized interacting with blood vessels. These tumors had mosaic vessels with focal regions in which no CD31- or CD105-expressing immunoreactivity was detected and cancer cells appeared to contact the vessel lumen. The

cancer cells appeared to form part of their own vasculature.³⁶ Transplantation of glioma cells expressing GFP in transgenic mice ubiquitously expressing RFP demonstrated that tumor-derived endothelial cells originated from tumor-initiating cells and did not result from cell fusion of endothelial cells and cancer cells. Thus cancer cells differentiated to endothelial cells which formed blood vessels within the tumor.³⁷

Cancer neurogenesis

In ND-GFP mice, GFP is expressed in nascent blood vessels and neural stem cells. A human intramedullary spinal cord tumor transplanted to ND-GFP nude mice attracted nestin-GFP cells expressing neuronal class III- β -tubulin as well as CD31 express cells. Both cell types surrounded the tumor. These results suggest that the tumor stimulated both neurogenesis as well as angiogenesis.³⁸

Imaging metastatic cells with GFP

The initial method used to introduce cancer cells into an animal model can affect the metastatic processes, with surgical orthotopic implantation (SOI) of tumor fragments resulting in the most patient-like model.³⁹

Imaging bone metastasis

A GFP-expressing MDA-MB-435 human breast carcinoma cell line produced widespread osteolytic skeletal metastases following injection into the left ventricle of the heart.⁴⁰ GFP expression also permitted *ex vivo* detection of single cells and microscopic metastases in bone at early time points.

Fragments of subcutaneously-growing H460-GFP lung tumors were implanted by SOI in the left lung of nude mice. Subsequent micrometastases were visualized by GFP fluorescence in the contralateral lung, plural membrane and widely throughout the skeletal system including the skull, vertebra, femur, tibia, pelvis and bone marrow of the femur and tibia.⁴¹

B16 GFP cells were i.v. injected in C57BL/6 mice and human LOX GFP melanoma cells intradermally injected in nude mice. Extensive bone and bone marrow metastases of B16F0 were visualized by GFP expression when the animals were sacrificed. Metastases for both cell lines were visualized in many organs, including the brain, lung, pleural membrane, liver, kidney, adrenal gland, lymph nodes, skeleton, muscle, and skin by GFP fluorescence.⁴²

The PC-3-GFP cells produced extensive bone lesions when injected into the tibia of immunocompromised mice. The skeletal progression of the PC-3 cells could be monitored by GFP optical imaging, X-ray, and by measurements of tumor products in serum, notably parathyroid hormone-related protein (PTHrP) and osteoprotegrin (OPG). The bisphosphonate, pamidronate, treatment reduced tumor burden as assessed by imaging and biomarkers.⁴³

Another bisphosphonate, 3,3-dimethylaminopropane-1-hydroxy-1,1-diphosphonic acid (olpadronate) was the most effective bisphosphonate treatment in reducing tumor burden as assessed by GFP imaging and radiography. The GFP tumor area and X-ray score

significantly correlated. Reduced tumor growth in the bone was accompanied by reduced serum calcium, PTHrP and OPG.⁴⁴

Human PC-3-GFP cells were transfected to express different forms of PTHrP and were injected intraskeletally. Skeletal progression of the prostate cancer cells was evaluated radiologically and by measurement of serum tumor markers. PTHrP transfection converted a non-invasive cell line into one that progressed in the skeleton: Injection of the PTHrP transfected cells resulted in greater tumor progression in bone when compared to non-transfected cells, and this effect was also influenced by non-amino terminal peptides of PTHrP.⁴⁵

Increased tumor progression was observed in PTHrP-overexpressing DU 145-GFP cells while decreased progression was observed in PTHrP-knockdown in PC-3-GFP cells. PTHrP-overexpressing DU 145 formed large tumors when implanted orthotopically into nude mice and resulted in spinal metastasis in one mouse, which was not observed in mice implanted with parental DU 145 cells. PTHrP-overexpressing DU 145 cells also caused significant bone destruction when injected into the tibiae of nude mice, unlike parental DU 145 cells.⁴⁶

Peyruchaud and colleagues⁴⁷ established a GFP-expressing bone-metastasis subclone of MDA-MB-231 breast cancer cells (B02/GFP.2) that grows preferentially in bone. Whole-body fluorescence imaging of the live mice showed that bone metastases could be detected about a week before radiologically distinctive osteolytic lesions developed. Furthermore, when the tumor-bearing mice were treated with a bisphosphonate, the progression of established osteolytic lesions and the expansion of the breast cancer cells in the bone were inhibited. Using whole-body GFP imaging, Peyruchaud et al.⁴⁸ also showed that the angiogenesis inhibitor angiostatin inhibited tumor growth in bone by inhibiting osteoclast activity.

Brain metastasis

In early experiments, the human lung adenocarcinoma cell-line Anip 973 was transfected with GFP and stable high-level GFP-expressing transfectants were established. GFP expressing cells were injected intravenously in nude mice as an experimental metastasis model. Intravenously injected mice had metastases in the brain and other organs as detected by GFP expression in fresh tissue.⁴⁹

In subsequent experiments, bright and highly stable GFP-expressing transfectants of the B16 mouse malignant melanoma cell line and the LOX human melanoma line were made. Metastases for both cell lines were visualized in many organs as described above, including the brain by GFP fluorescence.⁴²

PC-3 human prostate cancer growing orthotopically in nude mice formed micrometastases and metastases in the central nervous system in many organs, including the brain and spinal cord as visualized by GFP imaging.⁵⁰

Androgen-dependent variants of the LNCaP human prostate cancer which were more tumorigenic and exhibited invasive and metastatic compared to the parent LNCaP cells were

developed. Orthotopic transplantation of the androgen-independent variants of LNCaP expressing GFP resulted in multi-organ metastasis including the brain.⁵¹

Orthotopic transplantation of the murine Lewis lung carcinoma (LLC)-GFP resulted in rapid tumor growth in nude mice and extensive metastasis visualized by GFP-expression. Brain metastases were visualized in 30% of the animals.⁵²

Lewis lung carcinoma cells, stably expressing GFP, were injected in the chick embryo chorioallantoic membrane (CAM). GFP-Lewis lung carcinoma metastases were visualized by fluorescence, seven days additional incubation, in the brain and other organs, with the most frequent site being the brain.⁵³

An orthotopic retinoblastoma (RB) model was established with human RB cells expressing GFP. RB-GFP cells were injected into the subretinal space of nude mice. The growth of transplanted RB was observed *in vivo* using fluorescence stereomicroscopy. Metastasis to the cranium along the optic nerve was observed, with green fluorescent RB cells migrating along the optic nerve sheath and long posterior ciliary artery.⁵⁴

Two nasopharyngeal carcinoma cell lines stably expressing GFP, 5-8F-GFP and 6-10BGFP, were established. The cells were orthotopically injected into the nasopharynx. Whole-body fluorescence imaging was used to monitor the growth of the primary tumor as well as angiogenesis and metastasis which demonstrated brain metastasis of 5-8-F GFP. Cell line 6-10B was less metastatic, which occasionally resulted in pulmonary metastasis. GFP enabled imaging of micrometastasis. 5-8F was highly sensitive to 5-fluorouracil (5-FU), whereas 6-10B was moderately sensitive.⁵⁵

To develop an imageable, patient-like model of spinal cord glioma, U87 human glioma tumour fragments expressing RFP grown in nude mice were transplanted by SOI into the spinal cord of non-transgenic nude mice or transgenic nude mice expressing nestin-driven green fluorescent protein (ND-GFP) as described above. The intramedullary spinal cord tumour grew at the primary site, caused hind-limb paralysis and also metastasized to the brain.³⁸

Primary tumor size was significantly reduced by temozolomide treatment compared to untreated controls and brain metastases were found only in the control group. Histological analysis of the control group showed aggressive tumor invasion in the spinal cord. In contrast, temozolomide-treated animals showed mostly scar tissue after tumor transplantation.³⁸

Multiphoton laser scanning microscopy was used to image brain metastasis formation in real time at the single-cell level. Brain metastases arrested at vascular branch points and were closely associated with microvessels. Long-term dormancy was observed for some of the brain metastatic cells.⁵⁶

Estrogen-receptor (ER)-positive breast cancer cells expressing GFP, resistant to puromycin and non-tumorigenic without exogenous estrogen, were injected intracardially into mice that already had growing orthotopic tumors formed by ER-negative cells resistant to the

antibiotic G418. A variant cell line containing both estrogen-dependent and -independent cells was isolated from GFP expressing cells in the bone marrow, which was resistant to both puromycin and G418, suggesting its origin from the fusion of the two cells types. The fused cells were also metastatic to the brain detected by GFP, unlike parental cells. It was suggested that cell fusion can contribute to brain metastasis ability.⁵⁷

The effect of UVC irradiation was investigated on a model of experimental brain metastasis. For the brain metastasis model, lung cancer cells were injected intra-carotidally or stereotactically. The LLC line was used for the experimental brain metastasis model. The cancer cell were double-labeled with GFP in the nucleus and RFP in the cytoplasm. A craniotomy open window was used to image single cancer cells in the brain. The double-labeling of cancer cells with GFP and RFP enabled apoptosis of single cells to be imaged at the subcellular level through the craniotomy open window in live mice in real time. UVC irradiation, beamed through the craniotomy open window, induced apoptosis in the cancer cells. UVC irradiation was effective on LLC and significantly extended survival of the mice with experimental brain metastasis (Figure 2).⁵⁸

The dual-color LLC cells were imaged through the craniotomy open window 10 days after treatment with temozolomide. After treatment, dual-color cancer cells with fragmented nuclei were visualized, indicating apoptosis. GFP-expressing apoptotic bodies and the destruction of RFP-expressing cytoplasm were also visualized in real time in nude mice through the craniotomy open window.⁵⁹

Mitosis of the individual metastatic cancer cells on the brain were imaged dynamically in real time through the craniotomy open window. This model can be used to evaluate brain metastasis and brain cancer at the subcellular level including their sensitivity to currently used and experimental drugs (Figure 3).⁶⁰

BALB/c or SCID mice were injected intracardially with either 4T1-GFP or MDA231BRGFP breast cancer cells, and they subsequently formed brain metastasis. Antibody neutralization of either ALCAM or VLA-4 significantly reduced tumor seeding within the brain, suggesting that ALCAM/ALCAM and VLA-4/VCAM-1 interactions are important in the early stages of metastasis seeding in the brain.⁶¹

The mTOR inhibitor, rapamycin and Temsirolimus-CCI-779, inhibited brain metastasis of MDA-MB231-BR and CN34-BrM2 cancer cells expressing GFP.⁶² Sunitinib and dasatinib were visualized to inhibit brain metastases derived from human breast cancer 231BR cells expressing GFP.⁶³ 4T1-BrM5-GFP breast cancer cells administered into mammary fat pads of Balb/c mice subsequently formed brain metastasis. The substance P (SP) inhibitor spantide III decreased tumor cell colonization in the brain. SP inhibition in combination with other therapies may prevent breaching of the blood-brain barrier (BBB) by breast cancer cells and their colonization in the brain.⁶⁴ Sunitinib and dasatinib are multi-kinase inhibitors that may target metastasis.⁶³

Role of stroma and other host cells in metastasis

Human colon cancer cells that express GFP in the nucleus and RFP in the cytoplasm (HCT-116-GFP-RFP) were injected in either the portal vein (pv) or spleen of transgenic nude mice expressing GFP and imaged at the subcellular level *in vivo*. Extensive clasmocytosis (destruction of the cytoplasm) of the cancer cells occurred within 6 hours after pv injection and essentially all the cancer cells died. In contrast, splenic injection of these cancer cells resulted in the aggressive formation of liver and distant metastasis. GFP spleen cells were found in the liver metastases that resulted from intrasplenic injection of the cancer cells. When spleen cells and the cancer cells were co-injected in the pv, liver metastasis resulted that contained GFP spleen cells. These results suggest that the splenocytes are not just passengers but are required for liver metastasis.⁶⁵

Subsequent studies have shown that the metastatic cells can bring their own stromal components, including activated fibroblasts, from the primary site to the lungs. Viability of circulating metastatic cancer cells is higher if they are in emboli with stroma and have a growth advantage in the lung, confirming that stromal cells drive metastasis.⁶⁶

Human HCT-116-GFP-RFP colon cancer and mouse mammary tumor (MMT-RFP-GFP) cells were imaged in the pv of nude mice. Most HCT-116-GFP-RFP cells remained in sinusoids near peripheral portal veins. Only a small fraction of the cancer cells invaded the lobular area. Extensive clasmocytosis of the HCT-116-GFP-RFP cells occurred within 6 hours. Apoptosis was imaged in the dual-color cells by their altered nuclear morphology. In contrast, dual-color MMTGFP-RFP cells injected into the pv mostly survived in the liver of nude mice 24 hours after injection. The cells grew aggressively and formed colonies in the liver. However, when the host mice were pretreated with cyclophosphamide, the HCT-116-GFP-RFP cells also survived and formed colonies in the liver after pv injection. These results suggest that a cyclophosphamide-sensitive host cellular system attacked the HCT-116-GFP-RFP cells but could not effectively kill the MMT-GFP-RFP cells. This cyclophosphamide sensitive cellular system appears to inhibit metastasis of some cancer cell types and not others.⁶⁷

In another study that shows cyclophosphamide can drive metastasis, HT1080-GFP-RFP human fibrosarcoma cells with GFP in the nucleus and RFP in the cytoplasm were injected into the epigastric cranialis vein of nude mice. Twenty-four hours before cancer cell injection, cyclophosphamide was given i.p. and greatly increased metastasis of HT-1080 GFP-RFP cells. Cyclophosphamide seems to interfere with a host process that inhibits intravascular proliferation, extravasation, and extravascular colony formation which are important events in metastasis. Cyclophosphamide does not directly affect the cancer cells since cyclophosphamide has been cleared by the time the cancer cells were injected.⁶⁸

Identifying clonality of metastasis with GFP and RFP imaging

GFP-labeled and RFP-labeled HT-1080 human fibrosarcoma cells co-injected in the tail vein in order to determine clonality by fluorescence visualization of metastatic colonies. Pure red or pure green colonies were scored as clonal, whereas mixed red and green colonies were non-clonal. The clonality of the lung metastases was found to be dependent on the number

of cells injected. Spontaneous metastasis were often clonal and experimental metastasis are often non-clonal.^{4,69}

Imaging circulating tumor cells (CTCs) with GFP

GFP-expressing orthotopic PC-3 human prostate carcinomas produced viable circulating tumor cells (CTCs) but tumors of the same lineage did not when implanted subcutaneously. GFP-labeled circulating cells were more metastatic than the RFP-labeled parental cells when they were co-implanted in the prostate.⁷⁰

Mixtures of RFP- and GFP-expressing PC-3 human prostate carcinoma cells were implanted in the nude mouse prostate and metastasized. Yellow fluorescent PC-3 cells were observed and isolated from the circulation. The yellow fluorescent phenotype was heritable and stably maintained by cancer cells for many generations in vitro and in vivo. In the animals implanted with the yellow-fluorescing cells, 100% developed aggressive lung metastases. In contrast, when the GFP- and RFP-expressing parental cells were separately inoculated into the mouse prostate, none of the animals developed lung metastasis. All animals had almost exclusively yellow fluorescent cells in the blood and bone marrow. These results are consistent with the idea that spontaneous genetic exchange occurring between tumor cells in vivo contributes to genomic instability and creation of highly metastatic cells.⁷¹

In another study, using color-coded imaging of high-metastatic and low-metastatic osteosarcoma, it was observed that the high-metastatic phenotype could be transferred to the low-metastatic cells. The K-ras and possibly other genes were involved in conferring the high-metastatic phenotype.⁷²

Metastatic human prostate carcinoma cells selected for survival in the circulation have increased resistance to anoikis, which is apoptosis induced by cell detachment.⁷³

Using the GFP-expressing PC-3 orthotopic model and immunomagnetic beads coated with anti-epithelial cell adhesion molecule (EpCAM) and anti-prostate specific membrane antigen (PSMA), GFP-expressing CTC were isolated within 15 minutes and were readily visualized by GFP fluorescence. It was possible to immediately place the immunomagnetic-bead-captured GFP-expressing PC-3 CTCs in 3-dimensional sponge cell culture, where they proliferated.⁷⁴

The PC-3-GFP CTCs were then expanded in culture in parallel with the parental PC-3-GFP cell line. Both cell types were then inoculated onto the chorioallantoic membrane (CAM) of chick embryos. Eight days later, embryos were harvested and the brains were processed for frozen sections. The IV100 intravital laser scanning microscope enabled rapid identification of fluorescent metastatic foci within the chick embryonic brain. Inoculation of embryos with PC-3-GFP CTCs resulted in a 3- to 10-fold increase in brain metastasis when compared to those with the parental PC-3-GFP cells.⁷⁵

The PC-3-GFP CTC had a significantly increased sensitivity to both cisplatin and docetaxel when compared to PC-3 GFP parental cells, with docetaxel having the greater efficacy.⁷⁶

Imaging quiescent or dormant cancer cells

Fluorescent protein probes were developed, which label individual G_1 phase nuclei red and those in $S/G_2/M$ phases green. This system is called a fluorescence ubiquitous cell cycle indicator (FUCCI).⁷⁷

FUCCI 3D confocal imaging visualized that cancer cells in G_0/G_1 phase in Gelfoam[®] histoculture migrated more rapidly and further than cancer cells in $S/G_2/M$ phases. Cancer cells ceased migrating when they entered $S/G_2/M$ phases and restarted migrating after cell division when the cells re-entered G_0/G_1 . Migrating cancer cells also were resistant to cytotoxic chemotherapy, since they were preponderantly in G_0/G_1 , where cytotoxic chemotherapy is not effective (Figure 4).⁷⁸

FUCCI imaging showed that approximately 90% of cancer cells in the center and 80% of total cells of an established tumor are in G_0/G_1 phase. Similarly, approximately 75% of cancer cells far from ($> 100 \mu\text{m}$) tumor blood vessels of an established tumor are in G_0/G_1 . Longitudinal real-time imaging demonstrated that cytotoxic agents killed only proliferating cancer cells at the surface and, in contrast, had little effect on quiescent cancer cells, which are the vast majority of an established tumor. Moreover, resistant quiescent cancer cells restarted cycling after the cessation of chemotherapy (Figure 5).⁷⁹

FUCCI imaging demonstrated that OBP-301 adenovirus decoyed quiescent cancer cells to advance from G_0/G_1 to $S/G_2/M$ phases by mobilizing cell-cycle-related proteins. OBP-301 decoyed quiescent cancer stem-like cells in tumor spheres and also decoyed tumors *in vivo* into $S/G_2/M$ phases where they became chemosensitive.⁸⁰

Miyawaki et al.⁷⁷ utilized oscillating proteins to report cell-cycle transitions by linking them with a different colored fluorescent protein. These probes effectively label individual G_1 phase nuclei red and those in $S/G_2/M$ phase nuclei green.

Imageable color-coded tumor-host models

Dual-color fluorescence imaging can be effected by using RFP-expressing tumors growing in GFP-expressing transgenic mice. Tumor-stroma interaction, especially tumor-induced angiogenesis and tumor-infiltrating lymphocytes can be readily imaged in the model. GFP-expressing dendritic cells were observed contacting RFP-expressing tumor cells with their dendrites. GFP-expressing macrophages were observed engulfing RFP-expressing cancer cells. GFP lymphocytes were seen surrounding cells of the RFP tumor, which eventually regressed (Figure 6,7).⁸¹

HT-1080-GFP-RFP human fibrosarcoma cells were visualized surrounded by host-derived lymphocytes and macrophages both expressing GFP. It was possible to observe host GFP macrophages contacting, engulfing, and digesting dual-color HT-1080-GFP-RFP cells in real time. The dual-color cancer cells were readily visible after being engulfed in the GFP macrophages. Other cancer cells were visualized being killed by lymphocytes (Figure 8).⁸²

The Olympus IV100 Laser Scanning Microscope, with ultra-narrow microscope objectives (“stick objectives”), was used for non-invasive three-color whole-body imaging of the GFP-

RFP expressing cancer cells with GFP in the nucleus and RFP in the cytoplasm interacting with the GFP-expressing stromal cells in their transgenic nude mouse host footpad. In this model, drug response of both cancer and stromal cells in the intact live animal was also imaged in real time. Tumor-host interaction and cellular dynamics were imaged, including mitotic and apoptotic tumor cells, stromal cells interacting with the tumor cells, tumor vasculature, and tumor blood flow.⁸³

Human tumors grew extensively in nestin-driven (ND-GFP) nude mice. ND-GFP was shown to be highly expressed in proliferating endothelial cells and nascent blood vessels in the growing tumors, visualized by dual-color fluorescence imaging. Results of immunohistochemical staining showed that CD31 was expressed in the ND-GFP-expressing nascent blood vessels.⁸⁴

The tumor microenvironment (TME) has an important influence on tumor progression. Six different implantation models were developed to image the TME using multiple colors of fluorescent proteins: I) RFP- or GFP-expressing HCT-116 human colon cancer cells were implanted subcutaneously in the CFP-expressing nude mice. CFP stromal cells from the subcutaneous TME were visualized interacting with the RFP- or GFP-expressing tumors. II) RFP-expressing HCT-116 cells were transplanted into the spleen of CFP nude mice, which resulted in experimental metastases formed in the liver. CFP stromal cells from the liver TME were visualized interacting with the RFP-expressing tumor. III) RFP-expressing HCT-116 cancer cells were injected in the tail vein of CFP-expressing nude mice, forming experimental metastases in the lung. CFP stromal cells from the lung were visualized interacting with the RFP-expressing tumor. IV) In order to visualize two different tumors in the TME, GFP-expressing and RFP-expressing HCT-116 cancer cells were co-implanted subcutaneously in CFP-expressing nude mice. A 3-color TME was formed subcutaneously in the CFP mouse, and CFP stromal cells were visualized interacting with the RFP and GFP-expressing tumors. V) In order to have two different colors of stromal cells, GFP-expressing HCT-116 cells were initially injected subcutaneously in RFP-expressing nude mice. After 14 days, the tumor, which consisted of GFP cancer cells and RFP stromal cells derived from the RFP nude mouse, was harvested and transplanted into the CFP nude mouse. CFP stromal cells invaded the growing transplanted tumor containing GFP cancer cells and RFP stroma. VI) MMT cells expressing GFP in the nucleus and RFP in the cytoplasm were implanted in the spleen of a CFP nude mouse. Cancer cells were imaged in the liver 3 days after cell injection. The dual-color dividing MMT cells and CFP hepatocytes, as well as CFP non-parenchymal cells of the liver were imaged interacting with the 2-color cancer cells. CFP-expressing host cancer-associated fibroblasts (CAFs) (Figure 9) were predominantly observed in the TME models developed in the CFP nude mouse (Figure 10).⁸⁵

Non-colored HCT-116 human colon cancer cells were injected in the spleen of GFP nude mice which led to the formation of experimental liver metastasis. The TME of liver metastasis was imaged. GFP-expressing host cells were recruited by the metastatic tumors as visualized by fluorescence imaging. A desmin positive area increased around and within the liver metastasis over time, suggesting CAFs were recruited by the liver metastasis which have a role in tumor progression.⁸⁶

Tumor blood vessels when transplanted in nude mice along with a tumor, remained functional for more than 4 weeks after implantation suggesting long term persistence of stroma. Patient pancreatic tumors were passaged orthotopically in transgenic nude mice ubiquitously expressing RFP. The primary patient tumors acquired RFP-expressing stroma. The RFP-expressing stroma included CAFs and TAMs. Further passage to transgenic nude mice ubiquitously expressing GFP resulted in tumors that acquired GFP stroma in addition to their RFP stroma, including CAFs and TAMs as well as blood vessels. The RFP stroma persisted in the tumors growing in the GFP mice. Further passage to transgenic nude mice ubiquitously expressing CFP resulted in tumors acquiring CFP stroma in addition to persisting RFP and GFP stroma, including RFP- and GFP-expressing CAFs, TAMs and blood vessels.⁸⁷

After unlabeled primary patient tumors acquired GFP-expressing stroma by passage in GFP mice, subsequent liver metastases, and disseminated peritoneal metastases carried the stroma from the primary tumor, and recruited additional GFP-expressing stroma, resulting in the very bright fluorescence of the metastasis. The GFP-expressing stroma included CAFs and TAM in both the primary and metastatic tumors.⁸⁸

Patient pancreatic tumors previously passaged orthotopically into transgenic nude mice ubiquitously expressing GFP and subsequently to nude mice ubiquitously expressing RFP, where they acquired very bright GFP and RFP stroma, were then orthotopically passaged to nontransgenic nude mice. It was possible to image the brightly fluorescent tumors non-invasively longitudinally as they progressed in the non-transgenic nude mice (Figure 11).⁸⁹

Color-coding cancer stem cells and non-stem cells

The differential behavior of cancer stem-like and non-stem cells was simultaneously distinguished in the same tumor by real time by color-coded imaging. CD133⁺ Huh-7 human hepatocellular carcinoma (HCC) cells were considered as cancer stem-like cells (CSCs), and CD133⁻ Huh-7 cells were considered as non-stem cancer cells (NSCCs). CD133⁺ cells were labeled with GFP and CD133⁻ cells were labeled with RFP. GFP-CSCs were highly tumorigenic and metastatic as well as highly resistant to chemotherapy in vivo compared to RFP-NSCCs.⁹⁰

Use of fluorescent protein imaging to evaluate therapeutics

Human pancreatic cancer cell line MiaPaCa-2-RFP formed widespread metastases after orthotopic implants in mice. Gemcitabine (GEM) greatly improved survival by inducing transient tumor regression over the first 3 weeks. However, at this time, non-invasive imaging visualized tumor growth and dissemination occurred despite continued treatment, suggesting the development of tumor resistance to GEM. Drug efficacy was followed noninvasively in real time by imaging the RFP-expressing tumor and metastases, and was confirmed by fluorescent open imaging of autopsy specimens.⁹¹

Mice with orthotopic, MiaPaCa-2 RFP pancreatic cancer were then treated with GEM on a low metronomic dose schedule (METG) or maximum tolerated dose (MTDG) schedule with or without sunitinib (SU). Treatment with METG suppressed metastasis at multiple sites, an effect enhanced by SU.⁹²

Clinical application and potential clinical application of GFP imaging

The telomerase-specific replication-selective adenovirus expressing GFP (OBP-401) was able to detect viable human CTCs in peripheral blood ex vivo. The fluorescence signal was amplified only in viable, infected CTC by viral replication.⁹³ OBP-401-GFP labeled both epithelial and mesenchymal CTCs, providing a non-invasive alternative to tissue biopsy or surgical resection of primary tumours for companion diagnostics.⁹⁴

Fong et al.⁹⁵ used a herpes simplex virus (NV1066) vector that expresses the *gfp* gene to label, in a mouse model, metastatic lung tumor foci of less than 1 mm located in the pleural cavity. The tumor foci became fluorescent because NV1066 selectively replicates in cancer cells and expresses GFP. The fluorescently labeled tumors were detected by using a thoracoscopic endoscope system (which can be inserted into the thoracic cavity) equipped with fluorescent filters. Thus, fluorescent proteins have the potential as a tumor diagnosis.

Kishimoto et al.⁹⁶ selectively and accurately labeled existing tumors in mice with GFP using OBP-401 (Figure 12). The labeled tumors could then be resected under fluorescence guidance. Tumors that recurred after fluorescence-guided surgery maintained GFP expression.⁹⁷ Because the recurrent cancer cells stably express GFP, detection of cancer recurrence and metastasis is also possible with OBP-401 GFP labeling. Maintenance of label in recurrent tumors is not possible with nongenetic probes.⁹⁸

U87-RFP human glioma cells, expressing RFP, were injected stereotactically into the nude mouse brain through a craniotomy open window. Resulting gliomas were resected under fluorescence guidance or by bright light surgery (BLS). Almost all cancer cells were removed using fluorescence-guided navigation without damage to the brain tissue. In contrast, brain tumors were difficult to visualize under BLS and many residual cancer cells remained in the brain after bright-light surgery.⁹⁹

Human MiaPaCa-2-GFP pancreatic cancer cells were transplanted orthotopically in nude mice. BLS was performed on all tumor-bearing mice. The residual tumors were resected using a hand-held portable imaging system in mice treated with FGS. The surgical resection bed was irradiated with UVC. The average residual tumor area after FGS was significantly smaller than after BLS only. The BLS treated mice had significantly reduced survival compared to FGS- and FGS-UVC-treated mice for both relapse-free survival (RFS) and overall survival (OS). FGSUVC-treated mice had increased RFS and OS compared to FGS-only treated mice with RFS lasting at least 150 days, indicating the animals were cured.¹⁰⁰

New in vivo GFP imaging technology

Dual-color U87 human glioma and LLC cells, expressing GFP in the nucleus and RFP in the cytoplasm, were imaged through a craniotomy open window in nude mice. After treatment with temozolomide, dual-color cancer cells with fragmented nuclei were visualized, indicating apoptosis through the craniotomy window in live mice. GFP-expressing apoptotic bodies and the destruction of RFP-expressing cytoplasm were also visualized in live mice. Tumor volume in the treated group was significantly smaller than in the control group.⁵⁹ Mitosis of the individual cancer cells on the brain was also imaged dynamically in real time through the craniotomy-open window.⁶⁰ UVC irradiation, beamed through the craniotomy

open window, induced apoptosis in the cancer cells on the brain as imaged in live mice. UVC irradiation was effective on LLC and significantly extended survival of the mice with experimental brain metastasis. In contrast, the U87 glioma was relatively resistant to UVC irradiation.⁵⁸

In order to image the fate of cancer-cell-derived exosomes in orthotopic nude mouse models of breast cancer, GFP was linked to CD63, which is a general marker of exosomes. Orthotopic nude-mouse models of breast cancer engineered with CD63-GFP secreted exosomes into the tumor microenvironment. These results suggested that tumor-derived exosomes may contribute to forming a niche to promote tumor growth and metastasis.¹⁰¹

Human 143B osteosarcoma cells expressing α_v integrin-GFP were generated by transfection with an α_v integrin-GFP vector. Gelfoam[®] (5.5 mm) was transplanted subcutaneously in transgenic RFP nude mice. The implanted Gelfoam[®] became highly vascularized with RFP vessels. 143B cells expressing α_v integrin-GFP were injected into the vascularized Gelfoam[®]. Cancer cells and blood vessels were imaged in the vascularized Gelfoam[®] by color-coded confocal microscopy via a skin flap. Strong expression of α_v integrin-GFP in 143B cells was observed near RFP vessels in the Gelfoam[®].¹⁰²

When the 143B α_v integrin-GFP cells were orthotopically transplanted into the tibia of nude mice, the cells aligned along the collagen fibers within the tumor and had punctate expression of α_v integrin-GFP. Invading osteosarcoma cells had punctate α_v integrin-GFP in the muscle tissue at the primary tumor margin.¹⁰³

Using color-coded imaging, the interaction between GFP-expressing mesenchymal stromal cells (MSCs) and RFP-expressing 4T1 mouse mammary tumor cells was monitored. As few as five 4T1 cells could give rise to tumor formation when co-injected along with MSCs into the mouse mammary fat pad, but no tumor was formed when five or ten 4T1 cells were implanted alone. MSCs created a vascularized environment which enhances the ability of 4T1 cells to colonize and proliferate.¹⁰⁴

After tail vein injection of dual-color HT1080 RFP-GFP cancer cells, they could be imaged seeding and growing on the lung by open chest assisted-ventilation imaging. The seeding and arrest of single cancer cells on the lung, accumulation of cancer-cell emboli, cancer-cell viability, and metastatic colony formation were imaged in real-time by open-chest imaging.¹⁰⁵

Conclusions

Fluorescent proteins are the method of choice for whole-body imaging

The features of fluorescent-protein-based imaging, such as a very strong and stable signal, enable noninvasive whole-body imaging down to the subcellular level,⁸³ especially with red-shifted proteins, and make it far superior to luciferase-based imaging. Luciferase, with its very weak signal,¹⁰⁶ precluding image acquisition and allowing only photon counting with pseudocolor generated images, has very limited applications.¹⁰⁷ The luciferase reporter technique requires that animals are anesthetized and restrained so that sufficient photons can

be collected to construct a pseudo-image. Detection of luciferase labeled cells in vivo is very low resolution.¹ Therefore, cellular or subcellular imaging in vivo is not possible with luciferase. The dependence on circulating luciferin makes the signal from luciferase imaging unstable.¹⁰⁷ The luciferin substrate has to reach every tumor cell to be useful and the clearance of the luciferin results in an unstable signal.¹⁰⁸ This process must be carried out in an almost light-free environment. The requirement for photon counting using luciferase precludes real-time imaging. The one possible advantage of luciferase-based imaging is that no excitation light is necessary. However, far-red absorbing proteins such as Katushka greatly reduce problems with excitation, even in deep tissues, as shown by Shcherbo et al.² In comparison with the luciferase reporter, GFP has a much stronger signal and can therefore be used to image unrestrained animals down to the subcellular level with non-damaging blue light is only step. The RFP-signal was approximately 1,000 times stronger than that of the luciferase reporter.¹⁰⁶ Real-time images from fluorescent proteins in vivo can be captured using fairly simple apparatus and there is no need for total darkness.¹⁰⁸

In vivo GFP images can be captured using even an LED flashlight with a proper excitation filter and an emission filter with costs as low as several hundred dollars¹⁰ in comparison to hundreds of thousands of dollars worth of equipment necessary for luciferase imaging.

A novel fusion protein has been developed, ffLuc-cp156, which consists of a yellow variant of Aequorea GFP and firefly luciferase that yield a three orders of magnitude increase of photon yield over current luciferase systems and should prove to be very useful for in vivo imaging by allowing the advantages of both types of imaging simultaneously.¹¹⁰

Be careful of misconceptions in the literature. For example, the following was recently published “Whole animal fluorescence imaging in vivo suffers from low signal-to-noise as a result of background autofluorescence, modeling-dependent photon quantification, photobleaching, low tissue penetration, and low resolution”.¹¹¹ Despite enormous evidence to the contrary, as outlined above, this type of misinformation continues to be published even in 2013.

The GFP, RFP and CFP nude mice appear to have a life span similar to that of nontransgenic nude mice, such that longterm tumor growth and metastasis studies can be carried out.^{112, 113} Thus, fluorescent proteins are not toxic to the animal (Figure 13).

Non-invasive subcellular imaging⁸³ is a significant improvement from the inserted-window models¹⁶ or abdominal imaging windows¹¹⁴ or of the skin flap models we have previously developed to image tumors.^{13, 81}

Cell and tissue culture can be performed on different substrates such as on plastic, in Matrigel™, and on Gelfoam®, a sponge matrix. Each of these substrates consists of a very different surface, ranging from hard and inflexible, a gel, and a sponge-matrix, respectively. Folkman and Moscona found that cell shape was tightly coupled to DNA synthesis and cell growth. Therefore, the flexibility of a substrate is important for cells to maintain their optimal shape. Human osteosarcoma cells, stably expressing a fusion protein of $\alpha(v)$ integrin and green fluorescent protein (GFP), grew as a simple monolayer without any structure formation on the surface of a plastic dish. When the osteosarcoma cells were

cultured within Matrigel™, the cancer cells formed colonies but no other structures. When the cancer cells were seeded on Gelfoam®, the cells formed three-dimensional tissue-like structures. The behavior of 143B osteosarcoma cells on Gelfoam® in culture is remarkably different from those of these cells in monolayer culture or in Matrigel™. Tissue-like structures were observed only in Gelfoam® culture. The data in this report suggest a flexible structural substrate such as Gelfoam® provides a more in vivo-like culture condition than monolayer culture or Matrigel™ and that Matrigel™ does not result in actual three-dimensional culture (Figure 14).¹¹⁵

It is important to minimize autofluorescence of tissue and body fluids by using proper filters. Excitation filters should have a narrow band as close to 490 nm as possible to specifically excite GFP whose peak is distinct from that of the skin, tissues and fluid of the animal. In addition, proper band-pass emission filters should be used with a cutoff of approximately 515 nm.^{107, 116, 117}

Acknowledgments

These studies were supported in part by the National Cancer Institute grants CA132971 and CA142669 and CA183280.

References

1. Hoffman RM. The multiple uses of fluorescent proteins to visualize cancer in vivo. *Nature Reviews Cancer*. 2005; 5:796–806. [PubMed: 16195751]
2. Shcherbo D, Merzlyak EM, Chepurnykh TV, et al. Bright far-red fluorescent protein for whole-body imaging. *Nat Methods*. 2007; 4:741–746. [PubMed: 17721542]
3. Yang M, Baranov E, Wang JW, et al. Direct external imaging of nascent cancer, tumor progression, angiogenesis, and metastasis on internal organs in the fluorescent orthotopic model. *Proc Natl Acad Sci USA*. 2002; 99:3824–3829. [PubMed: 11891294]
4. Yamamoto N, Yang M, Jiang P, et al. Real-time imaging of individual color-coded metastatic colonies in vivo. *Clin Exp Metastasis*. 2003; 20:633–638. [PubMed: 14669794]
5. Brown EB, Campbell RB, Tsuzuki Y, et al. In vivo measurement of gene expression, angiogenesis and physiological function in tumors using multiphoton laser scanning microscopy. *Nature Med*. 2001; 7:864–868. [PubMed: 11433354]
6. Katz MH, Bouvet M, Takimoto S, et al. Survival efficacy of adjuvant cytosine-analogue CS-682 in a fluorescent orthotopic model of human pancreatic cancer. *Cancer Res*. 2004; 64:1828–1833. [PubMed: 14996746]
7. Verkhusha V, Lukyanov KA. The molecular properties and applications of Anthozoa fluorescent proteins and chromoproteins. *Nature Biotechnol*. 2004; 22:289–296. [PubMed: 14990950]
8. Chudakov DM, Matz MV, Lukyanov S, et al. Fluorescent proteins and their applications in imaging living cells and tissues. *Physiol Rev*. 2010; 90:1103–1163. [PubMed: 20664080]
9. Zimmer M. Green fluorescent protein (GFP): applications, structure and related photophysical behavior. *Chem Rev*. 2002; 102:759–781. [PubMed: 11890756]
10. Yang M, Luiken G, Baranov E, et al. Facile whole-body imaging of internal fluorescent tumors in mice with an LED flashlight. *Biotechniques*. 2005; 39:170–172. [PubMed: 16116787]
11. Yang M, Baranov E, Jiang P, et al. Whole-body optical imaging of green fluorescent protein-expressing tumors and metastases. *Proc Natl Acad Sci USA*. 2000; 97:1206–1211. [PubMed: 10655509]
12. Hiroshima Y, Maawy A, Sato S, et al. Hand-held high-resolution fluorescence imaging system for fluorescence-guided surgery of patient and cell-line pancreatic tumors growing orthotopically in nude mice. *J Surg Res*. 2014; 187:510–517. [PubMed: 24373959]

13. Yamauchi K, Yang M, Jiang P, et al. Development of real-time subcellular dynamic multicolor imaging of cancer cell-trafficking in live mice with a variable-magnification whole-mouse imaging system. *Cancer Res.* 2006; 66:4208–4214. [PubMed: 16618743]
14. Levenson R, Yang M, Hoffman RM. Whole-body dual-color differential fluorescence imaging of tumor angiogenesis enhanced by spectral unmixing. *Proc Am Assoc Cancer Res.* 2004; 45:46.
15. Chishima T, Miyagi Y, Wang X, et al. Cancer invasion and micrometastasis visualized in live tissue by green fluorescent protein expression. *Cancer Res.* 1997; 57:2042–2047. [PubMed: 9158003]
16. Jain RK, Munn LL, Fukumura D. Dissecting tumor pathophysiology using intravital microscopy. *Nature Rev Cancer.* 2002; 2:266–276. [PubMed: 12001988]
17. Naumov GN, Wilson SM, MacDonald IC, et al. Cellular expression of green fluorescent protein, coupled with high-resolution in vivo videomicroscopy, to monitor steps in tumor metastasis. *J Cell Sci.* 1999; 112:1835–1842. [PubMed: 10341203]
18. Farina KL, Wyckoff JB, Rivera J, et al. Cell motility of tumor cells visualized in living intact primary tumors using green fluorescent protein. *Cancer Res.* 1998; 58:2528–2532. [PubMed: 9635573]
19. Condeelis J, Segall JE. Intravital imaging of cell movement in tumors. *Nature Rev Cancer.* 2003; 3:921–930. [PubMed: 14737122]
20. Denk W, Strickler JH, Webb WW. Two-photon laser scanning fluorescence microscopy. *Science.* 1999; 248:73–76. [PubMed: 2321027]
21. Fukumura D, Yuan F, Monsky WL, et al. Effect of host microenvironment on the microcirculation of human colon adenocarcinoma. *Am J Pathol.* 1997; 151:679–688. [PubMed: 9284816]
22. Fukumura D, Xavier R, Sugiura T, et al. Tumor induction of VEGF promoter activity in stromal cells. *Cell.* 1998; 94:715–725. [PubMed: 9753319]
23. Amoh Y, Li L, Yang M, et al. Hair follicle-derived blood vessels vascularize tumors in skin and are inhibited by doxorubicin. *Cancer Res.* 2005; 65:2337–2343. [PubMed: 15781648]
24. Matsuzaki Y, Mabuchi Y, Okano H. Leptin receptor makes its mark on MSCs. *Cell Stem Cell.* 2014; 15:112–114. [PubMed: 25105573]
25. Chishima T, Miyagi Y, Wang X, et al. Metastatic patterns of lung cancer visualized live and in process by green fluorescent protein expression. *Clin Exp Metastasis.* 1997; 15:547–552. [PubMed: 9247257]
26. Huang MS, Wang TJ, Liang CL, et al. Establishment of fluorescent lung carcinoma metastasis model and its real-time microscopic detection in SCID mice. *Clin Exp Metastasis.* 2002; 19:359–368. [PubMed: 12090477]
27. Li CY, Shan S, Huang Q, et al. Initial stages of tumor cell-induced angiogenesis: evaluation via skin window chambers in rodent models. *J Natl Cancer Inst.* 2000; 92:143–147. [PubMed: 10639516]
28. Moore A, Marecos E, Simonova M, et al. Novel gliosarcoma cell line expressing green fluorescent protein: a model for quantitative assessment of angiogenesis. *Microvasc Res.* 1998; 56:145–153. [PubMed: 9828152]
29. Al-Mehdi AB, Tozawa K, Fisher AB, et al. Intravascular origin of metastasis from the proliferation of endothelium-attached tumor cells: a new model for metastasis. *Nature Med.* 2000; 6:100–102. [PubMed: 10613833]
30. Wong CW, Song C, Grimes MM, et al. Intravascular location of breast cancer cells after spontaneous metastasis to the lung. *Am J Pathol.* 2002; 161:749–753. [PubMed: 12213701]
31. Zhang Q, Yang M, Shen J, et al. The role of the intravascular microenvironment in spontaneous metastasis development. *Intl J Cancer.* 2010; 126:2534–2541.
32. Suetsugu A, Jiang P, Moriwaki H, et al. Imaging nuclear-cytoplasm dynamics of cancer cells in the intravascular niche of live mice. *Anticancer Res.* 2013; 33:4229–4236. [PubMed: 24122986]
33. Yamauchi K, Yang M, Jiang P, et al. Real-time in vivo dual-color imaging of intracapillary cancer cell and nucleus deformation and migration. *Cancer Res.* 2005; 65:4246–4252. [PubMed: 15899816]

34. Wolf K, te Lindert M, Krause M, et al. Physical limits of cell migration: Control by ECM space and nuclear deformation and tuning by proteolysis and traction force. *J Cell Biol.* 2013; 201:1069–1084. [PubMed: 23798731]
35. Hayashi K, Jiang P, Yamauchi K, et al. Real-time imaging of tumor-cell shedding and trafficking in lymphatic channels. *Cancer Res.* 2007; 67:8223–8228. [PubMed: 17804736]
36. Chang YS, di Tomaso E, McDonald DM, et al. Mosaic blood vessels in tumors: frequency of cancer cells in contact with flowing blood. *Proc Natl Acad Sci USA.* 2000; 97:14608–14613. [PubMed: 11121063]
37. Soda Y, Marumoto T, Friedmann-Morvinski D, et al. Transdifferentiation of glioblastoma cells into vascular endothelial cells. *Proc Natl Acad Sci USA.* 2011; 108:4274–4280. [PubMed: 21262804]
38. Hayashi K, Yamauchi K, Yamamoto N, et al. A color-coded orthotopic nude-mouse treatment model of brain-metastatic paralyzing spinal cord cancer that induces angiogenesis and neurogenesis. *Cell Proliferation.* 2009; 42:75–82. [PubMed: 19143765]
39. Hoffman RM. Orthotopic metastatic mouse models for anticancer drug discovery and evaluation: a bridge to the clinic. *Investigational New Drugs.* 1999; 17:343–359. [PubMed: 10759402]
40. Harms JF, Welch DR. MDA-MB-435 human breast carcinoma metastasis to bone. *Clin Exp Metastasis.* 2003; 20:327–334. [PubMed: 12856720]
41. Yang M, Hasegawa S, Jiang P, et al. Widespread skeletal metastatic potential of human lung cancer revealed by green fluorescent protein expression. *Cancer Res.* 1998; 58:4217–4221. [PubMed: 9766640]
42. Yang M, Jiang P, An Z, et al. Genetically fluorescent melanoma bone and organ metastasis models. *Clinical Cancer Res.* 1999; 5:3549–3559. [PubMed: 10589771]
43. Burton DW, Geller J, Yang M, et al. Monitoring of skeletal progression of prostate cancer by GFP imaging, X-ray, and serum OPG and PTHrP. *The Prostate.* 2005; 62:275–281. [PubMed: 15389781]
44. Yang M, Burton DW, Geller J, et al. The bisphosphonate olpadronate inhibits skeletal prostate cancer progression in a green fluorescent protein nude mouse model. *Clinical Cancer Res.* 2006; 12:2602–2606. [PubMed: 16638872]
45. Deftos LJ, Barken I, Burton DW, et al. Direct evidence that PTHrP expression promotes prostate cancer progression in bone. *Biochem Biophys Res Commun.* 2005; 327:468–472. [PubMed: 15629138]
46. Ongkeko WM, Burton D, Kiang A, et al. Parathyroid hormone related-protein promotes epithelial-to-mesenchymal transition in prostate cancer. *PLoS One.* 2014; 9:e85803. [PubMed: 24465715]
47. Peyruchaud O, Winding B, Pécheur I, et al. Early detection of bone metastases in a murine model using fluorescent human breast cancer cells: application to the use of the bisphosphonate zoledronic acid in the treatment of osteolytic lesions. *J Bone Miner Res.* 2001; 16:2027–2034. [PubMed: 11697798]
48. Peyruchaud O, Serre CM, NicAmhlaioibh R, et al. Angiostatin inhibits bone metastasis formation in nude mice through a direct anti-osteoclastic activity. *J Biol Chem.* 2003; 278:45826–45832. [PubMed: 12954626]
49. Chishima T, Miyagi Y, Wang X, et al. Visualization of the metastatic process by green fluorescent protein expression. *Anticancer Res.* 1997; 17:2377–2384. [PubMed: 9252650]
50. Yang M, Jiang P, Sun FX, et al. A fluorescent orthotopic bone metastasis model of human prostate cancer. *Cancer Res.* 1999; 59:781–786. [PubMed: 10029062]
51. Tso CL, McBride WH, Sun J, et al. Androgen deprivation induces selective outgrowth of aggressive hormone-refractory prostate cancer clones expressing distinct cellular and molecular properties not present in parental androgen-dependent cancer cells. *Cancer J.* 2000; 6:220–233. [PubMed: 11038142]
52. Rashidi B, Yang M, Jiang P, et al. A highly metastatic Lewis lung carcinoma orthotopic green fluorescent protein model. *Clin Exp Metastasis.* 2000; 18:57–60. [PubMed: 11206839]
53. Bobek V, Plachy J, Pinterova D, et al. Development of a green fluorescent protein metastatic-cancer chick-embryo drug-screen model. *Clin Exp Metastasis.* 2004; 21:347–352. [PubMed: 15554391]

54. Wang XL, Xu P, Wang F, et al. A new orthotopic retinoblastoma model expressing green fluorescent protein. *Zhonghua Yan Ke Za Zhi*. 2004; 40:225–228. [PubMed: 15268827]
55. Liu T, Ding Y, Xie W, et al. An imageable metastatic treatment model of nasopharyngeal carcinoma. *Clin Cancer Res*. 2007; 13:3960–3967. [PubMed: 17606730]
56. Kienast Y, von Baumgarten L, Fuhrmann M, et al. Real-time imaging reveals the single steps of brain metastasis formation. *Nature Med*. 2010; 16:116–122. [PubMed: 20023634]
57. Mukhopadhyay KD, Bandyopadhyay A, Chang TT, et al. Isolation and characterization of a metastatic hybrid cell line generated by ER negative and ER positive breast cancer cells in mouse bone marrow. *PLoS One*. 2011; 6:e20473. [PubMed: 21673810]
58. Momiyama M, Suetsugu A, Kimura H, et al. Imaging the efficacy of UVC irradiation on superficial brain tumors and metastasis in live mice at the subcellular level. *J Cell Biochem*. 2013; 114:428–434. [PubMed: 22961687]
59. Momiyama M, Suetsugu A, Chishima T, et al. Subcellular real-time imaging of the efficacy of temozolomide on cancer cells in the brain of live mice. *Anticancer Res*. 2013; 33:103–106. [PubMed: 23267133]
60. Momiyama M, Suetsugu A, Kimura H, et al. Dynamic subcellular imaging of cancer cell mitosis in the brain of live mice. *Anticancer Res*. 2013; 33:1367–1372. [PubMed: 23564774]
61. Soto MS, Serres S, Anthony DC, et al. Functional role of endothelial adhesion molecules in the early stages of brain metastasis. *Neuro Oncology*. 2014; 16:540–551. [PubMed: 24311639]
62. Zhao H, Cui K, Nie F, et al. The effect of mTOR inhibition alone or combined with MEK inhibitors on brain metastasis: an in vivo analysis in triple-negative breast cancer models. *Breast Cancer Res Treat*. 2012; 131:425–436. [PubMed: 21394501]
63. Zhao H, Jin G, Cui K, et al. Novel modeling of cancer cell signaling pathways enables systematic drug repositioning for distinct breast cancer metastases. *Cancer Res*. 2013; 73:6149–6163. [PubMed: 24097821]
64. Rodriguez PL, Jiang S, Fu Y, et al. The proinflammatory peptide substance P promotes blood–brain barrier breaching by breast cancer cells through changes in microvascular endothelial cell tight junctions. *Int J Cancer*. 2014; 134:1034–1044. [PubMed: 23934616]
65. Bouvet M, Tsuji K, Yang M, et al. In vivo color-coded imaging of the interaction of colon cancer cells and splenocytes in the formation of liver metastases. *Cancer Res*. 2006; 66:11293–11297. [PubMed: 17145875]
66. Duda DG, Duyverman AM, Kohno M, et al. Malignant cells facilitate lung metastasis by bringing their own soil. *Proc Natl Acad Sci USA*. 2010; 107:21677–21682. [PubMed: 21098274]
67. Tsuji K, Yamauchi K, Yang M, et al. Dual-color imaging of nuclear-cytoplasmic dynamics, viability, and proliferation of cancer cells in the portal vein area. *Cancer Res*. 2006; 66:303–306. [PubMed: 16397243]
68. Yamauchi K, Yang M, Hayashi K, et al. Induction of cancer metastasis by cyclophosphamide pretreatment of host mice: an opposite effect of chemotherapy. *Cancer Res*. 2008; 68:516–520. [PubMed: 18199547]
69. Yamamoto N, Yang M, Jiang P, et al. Determination of clonality of metastasis by cell-specific color-coded fluorescent-protein imaging. *Cancer Res*. 2003; 63:7785–7790. [PubMed: 14633704]
70. Glinskii AB, Smith BA, Jiang P, et al. Viable circulating metastatic cells produced in orthotopic but not ectopic prostate cancer models. *Cancer Res*. 2003; 63:4239–4243. [PubMed: 12874032]
71. Glinsky GV, Glinskii AB, Berezovskaya O, et al. Dual-color-coded imaging of viable circulating prostate carcinoma cells reveals genetic exchange between tumor cells in vivo, contributing to highly metastatic phenotypes. *Cell Cycle*. 2006; 5:191–197. [PubMed: 16357534]
72. Tome Y, Tsuchiya H, Hayashi K, et al. In vivo gene transfer between interacting human osteosarcoma cell lines is associated with acquisition of enhanced metastatic potential. *J Cell Biochem*. 2009; 108:362–367. [PubMed: 19623575]
73. Berezovskaya O, Schimmer AD, Glinskii AB, et al. Increased expression of apoptosis inhibitor protein XIAP contributes to anoikis resistance of circulating human prostate cancer metastasis precursor cells. *Cancer Res*. 2005; 65:2378–2386. [PubMed: 15781653]

74. Kolostova K, Pinterova D, Hoffman RM, et al. Circulating human prostate cancer cells from an orthotopic mouse model rapidly captured by immunomagnetic beads and imaged by GFP expression. *Anticancer Res.* 2011; 31:1535–1539. [PubMed: 21617207]
75. Menen RS, Pinney E, Kolostova K, et al. A rapid imageable in vivo metastasis assay for circulating tumor cells. *Anticancer Res.* 2011; 31:3125–3128. [PubMed: 21965717]
76. Menen R, Zhao M, Zhang L, et al. Comparative chemosensitivity of circulating human prostate cancer cells and primary cancer cells. *Anticancer Res.* 2012; 32:2881–2884. [PubMed: 22753751]
77. Sakaue-Sawano A, Kurokawa H, Morimura T, et al. Visualizing Spatiotemporal Dynamics of Multicellular Cell-Cycle Progression. *Cell.* 2008; 132:487–498. [PubMed: 18267078]
78. Yano S, Miwa S, Mii S, et al. Invading cancer cells are predominantly in G₀/G₁ resulting in chemoresistance demonstrated by real-time FUCCI imaging. *Cell Cycle.* 2014; 13:953–960. [PubMed: 24552821]
79. Yano S, Zhang Y, Miwa S, et al. Spatial-temporal FUCCI imaging of each cell in a tumor demonstrates locational dependence of cell cycle dynamics and chemoresponsiveness. *Cell Cycle.* 2014; 13:2110–2119. [PubMed: 24811200]
80. Yano S, Tazawa H, Hashimoto Y, et al. A genetically engineered oncolytic adenovirus decoys and lethally traps quiescent cancer stem-like cells into S/G₂/M phases. *Clin Cancer Res.* 2013; 19:6495–6505. [PubMed: 24081978]
81. Yang M, Li L, Jiang P, et al. Dual-color fluorescence imaging distinguishes tumor cells from induced host angiogenic vessels and stromal cells. *Proc Natl Acad Sci USA.* 2003; 100:14259–14262. [PubMed: 14614130]
82. Yamauchi K, Tome Y, Yamamoto N, et al. Color-coded real-time subcellular fluorescence imaging of the interaction between cancer and host cells in live mice. *Anticancer Res.* 2012; 32:39–44. [PubMed: 22213286]
83. Yang M, Jiang P, Hoffman RM. Whole-body subcellular multicolor imaging of tumor-host interaction and drug response in real time. *Cancer Res.* 2007; 67:5195–5199. [PubMed: 17545599]
84. Amoh Y, Yang M, Li L, et al. Nestin-linked green fluorescent protein transgenic nude mouse for imaging human tumor angiogenesis. *Cancer Res.* 2005; 65:5352–5357. [PubMed: 15958583]
85. Suetsugu A, Hassanein MK, Reynoso J, et al. The cyan fluorescent protein nude mouse as a host for multicolor-coded imaging models of primary and metastatic tumor microenvironments. *Anticancer Res.* 2012; 32:31–38. [PubMed: 22213285]
86. Suetsugu A, Osawa Y, Nagaki M, et al. Imaging the recruitment of cancer-associated fibroblasts by liver-metastatic colon cancer. *J Cell Biochem.* 2011; 112:949–953. [PubMed: 21328469]
87. Suetsugu A, Katz M, Fleming J, et al. Multi-color palette of fluorescent proteins for imaging the tumor microenvironment of orthotopic tumorgraft mouse models of clinical pancreatic cancer specimens. *J Cell Biochem.* 2012; 113:2290–2295. [PubMed: 22573550]
88. Suetsugu A, Katz M, Fleming J, et al. Imageable fluorescent metastasis resulting in transgenic GFP mice orthotopically implanted with human-patient primary pancreatic cancer specimens. *Anticancer Res.* 2012; 32:1175–1180. [PubMed: 22493347]
89. Suetsugu A, Katz M, Fleming J, et al. Non-invasive fluorescent-protein imaging of orthotopic pancreatic-cancer-patient tumorgraft progression in nude mice. *Anticancer Res.* 2012; 32:3063–3068. [PubMed: 22843874]
90. Suetsugu S, Osawa Y, Nagaki M, et al. Simultaneous color-coded imaging to distinguish cancer “stem-like” and non-stem cells in the same tumor. *J Cell Biochem.* 2010; 111:1035–1041. [PubMed: 20672309]
91. Katz M, Takimoto S, Spivac D, et al. A novel red fluorescent protein orthotopic pancreatic cancer model for the preclinical evaluation of chemotherapeutics. *J Surg Res.* 2003; 113:151–160. [PubMed: 12943825]
92. Tran Cao HS, Bouvet M, Kaushal S, et al. Metronomic gemcitabine in combination with Sunitinib inhibits multisite metastasis and increases survival in an orthotopic model of pancreatic cancer. *Mol Cancer Therap.* 2010; 9:2068–2078. [PubMed: 20606044]
93. Kojima T, Hashimoto Y, Watanabe Y, et al. A simple biological imaging system for detecting viable human circulating tumor cells. *J Clin Invest.* 2009; 119:3172–3181. [PubMed: 19729837]

94. Shigeyasu K, Tazawa H, Hashimoto Y, et al. Fluorescence virus-guided capturing system of human colorectal circulating tumour cells for non-invasive companion diagnostics. *Gut*. 2014 May 28. pii: gutjnl-2014-306957. Epub ahead of print. 10.1136/gutjnl-2014-306957
95. Stiles BM, Adusumilli PS, Bhargava A, et al. Minimally invasive localization of oncolytic herpes simplex viral therapy of metastatic pleural cancer. *Cancer Gene Ther*. 2006; 13:53–64. [PubMed: 16037824]
96. Kishimoto H, Zhao M, Hayashi K, et al. In vivo internal tumor illumination by telomerase-dependent adenoviral GFP for precise surgical navigation. *Proc Natl Acad Sci USA*. 2009; 106:14514–14517. [PubMed: 19706537]
97. Kishimoto H, Aki R, Urata Y, et al. Tumor-selective, adenoviral-mediated GFP genetic labeling of human cancer in the live mouse reports future recurrence after resection. *Cell Cycle*. 2011; 10:2737–2741. [PubMed: 21785265]
98. Bouvet M, Hoffman RM. Glowing tumors make for better detection and resection. *Sci Transl Med*. 2011; 3:110fs10.
99. Momiyama M, Hiroshima Y, Suetsugu A, et al. Enhanced resection of orthotopic red-fluorescent-protein-expressing human glioma by fluorescence-guided surgery in nude mice. *Anticancer Res*. 2013; 33:107–111. [PubMed: 23267134]
100. Hiroshima Y, Maawy A, Zhang Y, et al. Fluorescence-guided surgery in combination with UVC irradiation cures metastatic human pancreatic cancer in orthotopic mouse models. *PLoS One*. 2014; 9:e99977. [PubMed: 24924955]
101. Suetsugu A, Honma K, Saji S, et al. Imaging exosome transfer from breast cancer cells to stroma at metastatic sites in orthotopic nude mouse models. *Adv Drug Deliv Rev*. 2013; 65:383–390. [PubMed: 22921594]
102. Uehara F, Tome Y, Yano S, et al. A color-coded imaging model of the interaction of α_v integrin-GFP expressed in osteosarcoma cells and RFP expressing blood vessels in Gelfoam® vascularized in vivo. *Anticancer Res*. 2013; 33:1361–1366. [PubMed: 23564773]
103. Tome Y, Sugimoto N, Yano S, et al. Real-time imaging of α_v integrin molecular dynamics in osteosarcoma cells in vitro and in vivo. *Anticancer Res*. 2013; 33:3021–3025. [PubMed: 23898055]
104. Ke CC, Liu RS, Suetsugu A, et al. In vivo fluorescence imaging reveals the promotion of mammary tumorigenesis by mesenchymal stromal cells. *PLoS One*. 2013; 8:e69658. [PubMed: 23936067]
105. Kimura H, Hayashi K, Yamauchi K, et al. Real-time imaging of single cancer-cell dynamics of lung metastasis. *J Cell Biochem*. 2010; 109:58–64. [PubMed: 19911396]
106. Ray P, De A, Min JJ, et al. Imaging tri-fusion multimodality reporter gene expression in living subjects. *Cancer Res*. 2004; 64:1323–1330. [PubMed: 14973078]
107. Hoffman RM, Yang M. Whole-body imaging with fluorescent proteins. *Nat Protoc*. 2006; 1:1429–1438. [PubMed: 17406431]
108. Burgos JS, Rosol M, Moats RA, et al. Time course of bioluminescent signal in orthotopic and heterotopic brain tumors in nude mice. *Biotechniques*. 2003; 34:1184–1188. [PubMed: 12813886]
109. Hoffman, RM. Fluorescent proteins as visible in vivo sensors. In: Morris, May C., editor. *Progress in Molecular Biology and Translational Science*. Vol. 113. Burlington: Academic Press; 2013. p. 389-402.
110. Hara-Miyauchi C, Tsuji O, Hanyu A, et al. Bioluminescent system for dynamic imaging of cell and animal behavior. *Biochem Biophys Res Commun*. 2012; 419:188–193. [PubMed: 22333570]
111. Kocher B, Piwnica-Worms D. Illuminating cancer systems with genetically engineered mouse models and coupled luciferase reporters in vivo. *Cancer Disc*. 2013; 3:616–629.
112. Yang M, Reynoso J, Jiang P, et al. Transgenic nude mouse with ubiquitous green fluorescent protein expression as a host for human tumors. *Cancer Res*. 2004; 64:8651–8656. [PubMed: 15574773]
113. Yang M, Reynoso J, Bouvet M, et al. A transgenic red fluorescent protein-expressing nude mouse for color-coded imaging of the tumor microenvironment. *J Cell Biochem*. 2009; 106:279–284. [PubMed: 19097136]

114. Ritsma L, Steller EJ, Beerling E, et al. Intravital microscopy through an abdominal imaging window reveals a pre-micrometastasis stage during liver metastasis. *Sci Transl Med.* 2012; 4:158ra145.
115. Tome Y, Uehara F, Mii S, et al. 3-dimensional tissue is formed from cancer cells in vitro on Gelfoam[®], but not on Matrigel[™]. *J Cell Biochem.* 2014; 115:1362–1367. [PubMed: 24497277]
116. Hoffman RM, Yang M. Subcellular imaging in the live mouse. *Nat Protoc.* 2006; 1:775–782. [PubMed: 17406307]
117. Hoffman RM, Yang M. Color-coded fluorescence imaging of tumor–host interactions. *Nat Protoc.* 2006; 1:928–935. [PubMed: 17406326]

Article Features

1. Cancer cells can be stably transfected with fluorescent proteins that brightly fluoresce *in vitro* as well as *in vivo*.
2. Tumors and metastases that express fluorescent proteins can be visualized noninvasively in intact animals, including deep set tumors, using techniques such as spectral separation.
3. For single-cell imaging on deep organs, reversible skin-flaps and chronic windows with or without an implanted device can be used.
4. The cell cycle of single cancer cells, including dormancy, can be imaged using fluorescent proteins linked to cell cycle-specific proteins.
5. Subcellular imaging *in vivo* can be achieved with cancer cells which express two or more different-colored fluorescent proteins. For example, the nucleus can be labeled with green fluorescent protein and the cytoplasm with red fluorescent protein. This enables nuclear–cytoplasmic dynamics to be visualized *in vivo*, including mitosis and apoptosis. Subcellular imaging can be achieved noninvasively depending on the location.
6. Transgenic mice can express a fluorescent protein in almost all cells or in specific cells, depending on how the fluorescent protein gene is linked. Colored mice can be transplanted with tumors expressing different-colored fluorescent proteins to create a dual-color image of the tumor–host interaction. Transplantation of cells from different colored mice to along with dual-colored cancer cells can be used to make a multiple-colored model *in vivo* model of interaction. Transgenic colored nude mice are very appropriate for the growth of human tumors.
7. *In vivo* fluorescence imaging can be used to visualize the efficacy of candidate cancer drugs in real time in mouse models of human cancer, including differential activity on primary cancer and metastasis and stroma cells at the single-cell level.
8. Fluorescent proteins can be used for ‘molecular imaging’ to visualize the effects of single-gene changes — for example, on cancer metastasis or drug sensitivity. Specific proteins linked to a fluorescent protein can also be imaged *in vivo*.
9. Future uses of fluorescent proteins in human cancer diagnosis and therapy are possible — for example, for fluorescence-guided surgery in mouse models, since tumors can be selectively and stably transformed *in vivo* with a fluorescent protein by viral vectors.
10. Fluorescent protein imaging has significant advantages over luciferase photon counting, including brighter signals, orders of magnitude higher resolution, substrate independence, availability in multiple colors, and simpler and cheaper equipment requirements.

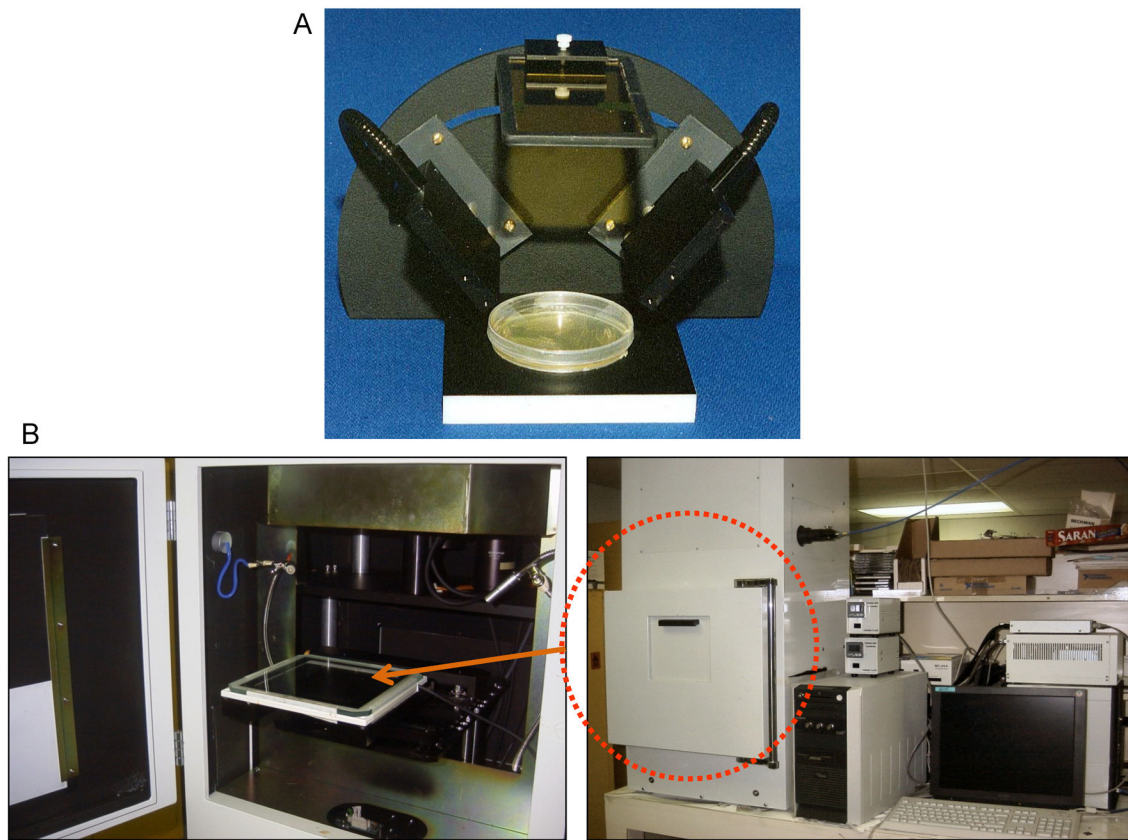


Figure 1.

an example of the earliest prototype for in vivo imaging with GFP is the Illumatool a simple instrument with a light sources that are properly filtered to avoid autofluorescence and an emission filter through which it is possible to image GFP fluorescence from unrestrained animals.¹¹ An example of the best state of the art, OV100 small animal imaging system: The OV-100 Small Animal Imaging System (Olympus, Tokyo, Japan), containing an MT-20 light source (Olympus) and DP70 CCD camera (Olympus) was used. The optics of the OV-100 fluorescence imaging system have been specially developed for macroimaging as well as microimaging with high light-gathering capacity. The instrument incorporates a unique combination of high numerical aperture and long working distance. Five individually optimized objective lenses, parcentered and parfocal, provide a 105-fold magnification range for seamless imaging of the entire body down to the subcellular level without disturbing the animal. The OV-100 has the lenses mounted on an automated turret with a high magnification range of $\times 1.6$ to $\times 16$ and a field of view ranging from 6.9 to 0.69 mm. The optics and antireflective coatings ensure optimal imaging of multiplexed fluorescent reporters in small animals. High-resolution images were captured directly on a PC (Fujitsu Siemens, Munich, Germany). Images were processed for contrast and brightness and analyzed with the use of Paint Shop Pro 8 and CellR (Olympus Biosystems).¹³

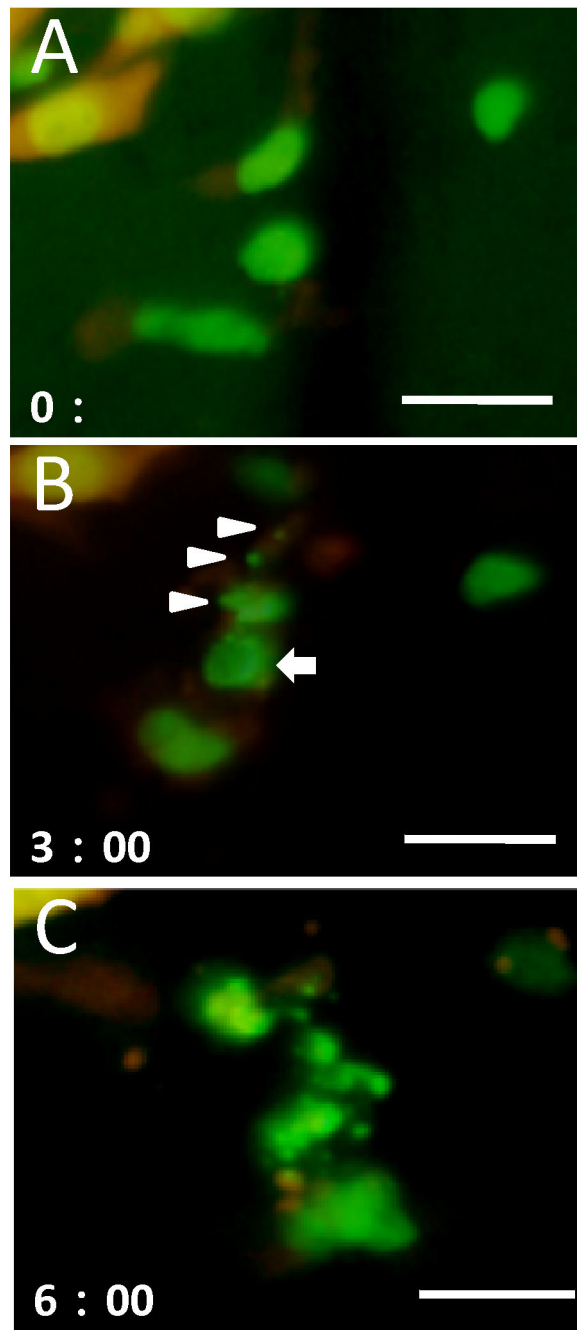


Figure 2. Real-time imaging of apoptotic cell death in the brain in live mice

(A) Seven days after dual-color Lewis lung carcinoma (LLC) cell inoculation via the internal carotid artery, the cells were irradiated for 60 s with UVC. (B) Three hours after irradiation, aggregation of chromatin at the nuclear membrane (arrow) and fragmented nuclei (arrow heads) were observed. (C) Six hours after irradiation, the nuclei appeared to form numerous additional fragments and destruction of RFP-expressing cytoplasm was observed (scale bars, a,b: 100 mm; c: 20 mm).⁵⁸

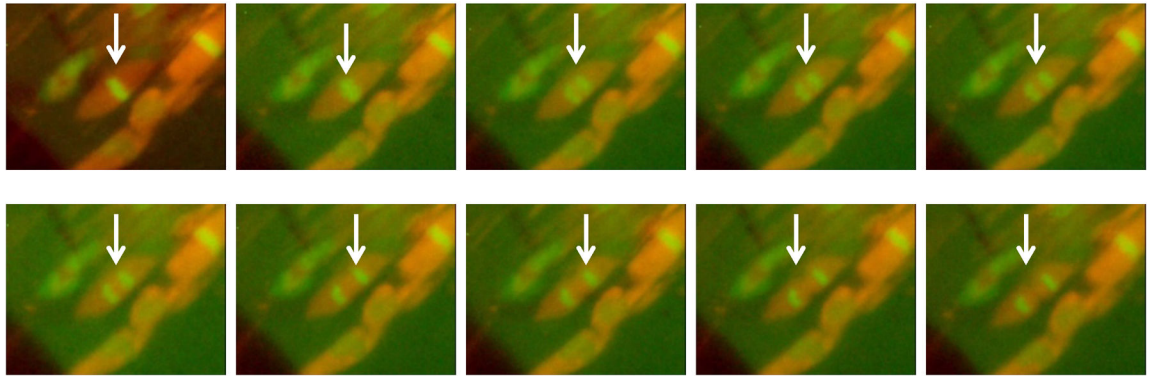


Figure 3. Time-course dynamic imaging of a dual-color Lewis lung carcinoma (LLC) cell undergoing mitosis in the brain visualized through the craniotomy window with the OV100 imaging system. Arrows point to the same cell undergoing mitosis.⁶⁰

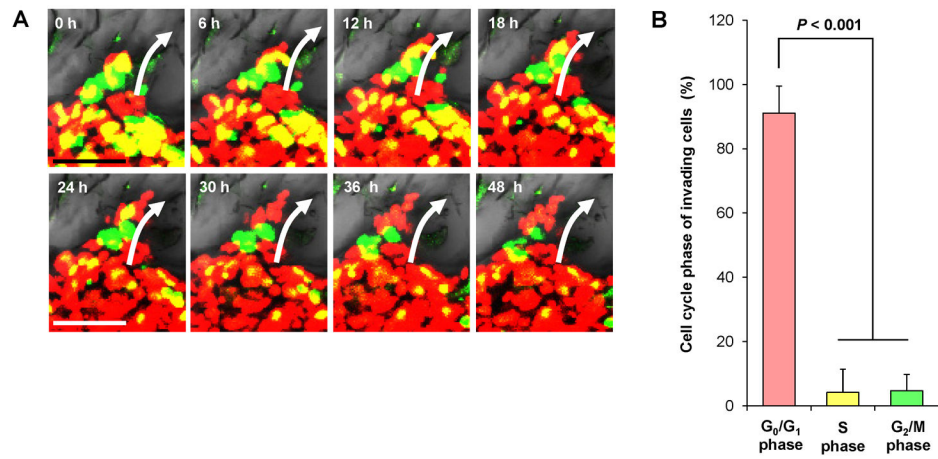


Figure 4. Invasive cancer cells are predominantly in G₀/G₁
 FUCCI-expressing cancer cells (5×10^6) were placed on Gelfoam[®] (1×1 cm) in RPMI 1640 medium. **(A)** High-magnification real-time images of invading cancer cells cultured on Gelfoam[®] for 48 h. Arrows show the direction of invading cancer cells. **(B)** Histogram shows cell cycle phase of invading cancer cells.⁷⁸

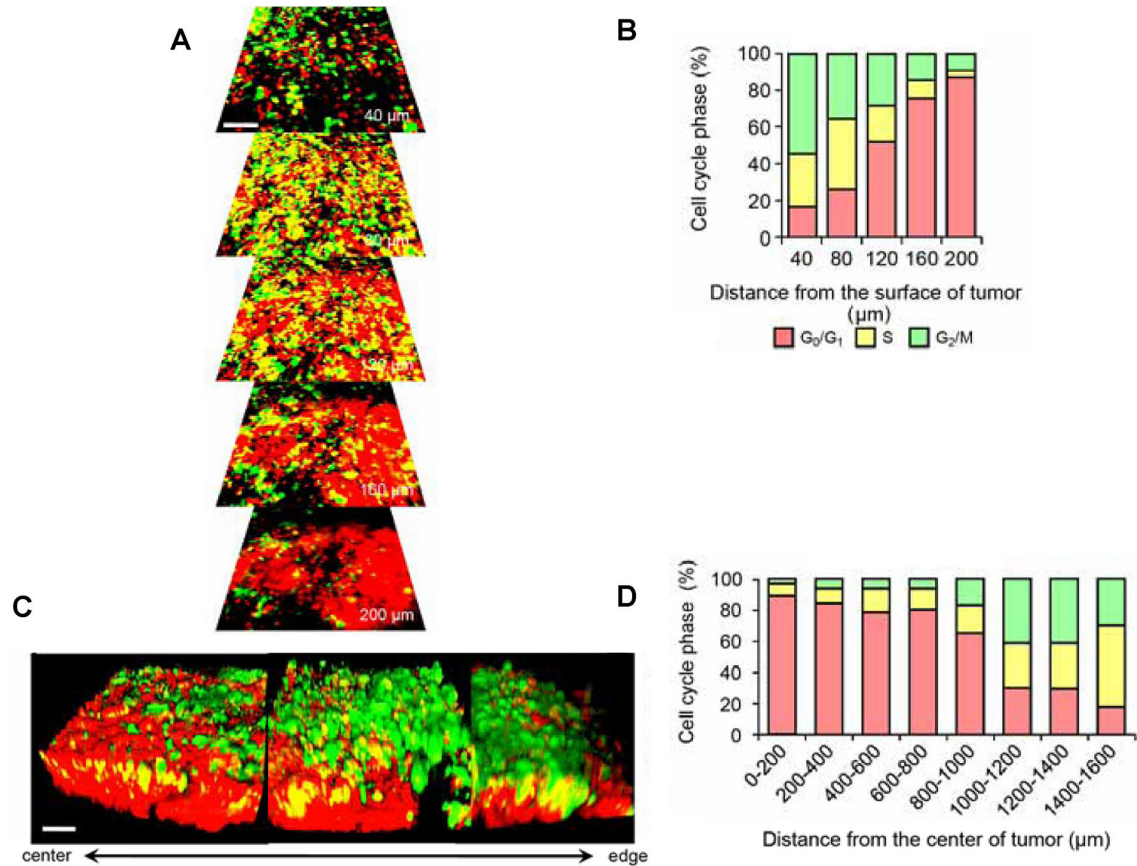


Figure 5. Cell cycle phase distribution of cancer cells at the tumor surface and center (A) Fucci-expressing MKN45 cells were implanted directly in the liver of nude mice and imaged at 35 d. (B) Histogram shows the cell cycle distribution in the tumor at 35 d after implantation. (C) Representative 3D reconstruction images of a nascent tumor at 35 d after implantation. (D) Histogram shows the distribution of Fucci-expressing cells at different distances from the center. The number of cells in each cell cycle phase were assessed by counting the number of cells of each color at the indicated time points and depth. The percentages of cells in the G₂/M, S, and G₀/G₁ phases of the cell cycle are shown (D). Data are means (each group for n = 5). Scale bars represent 100 μm .⁷⁹

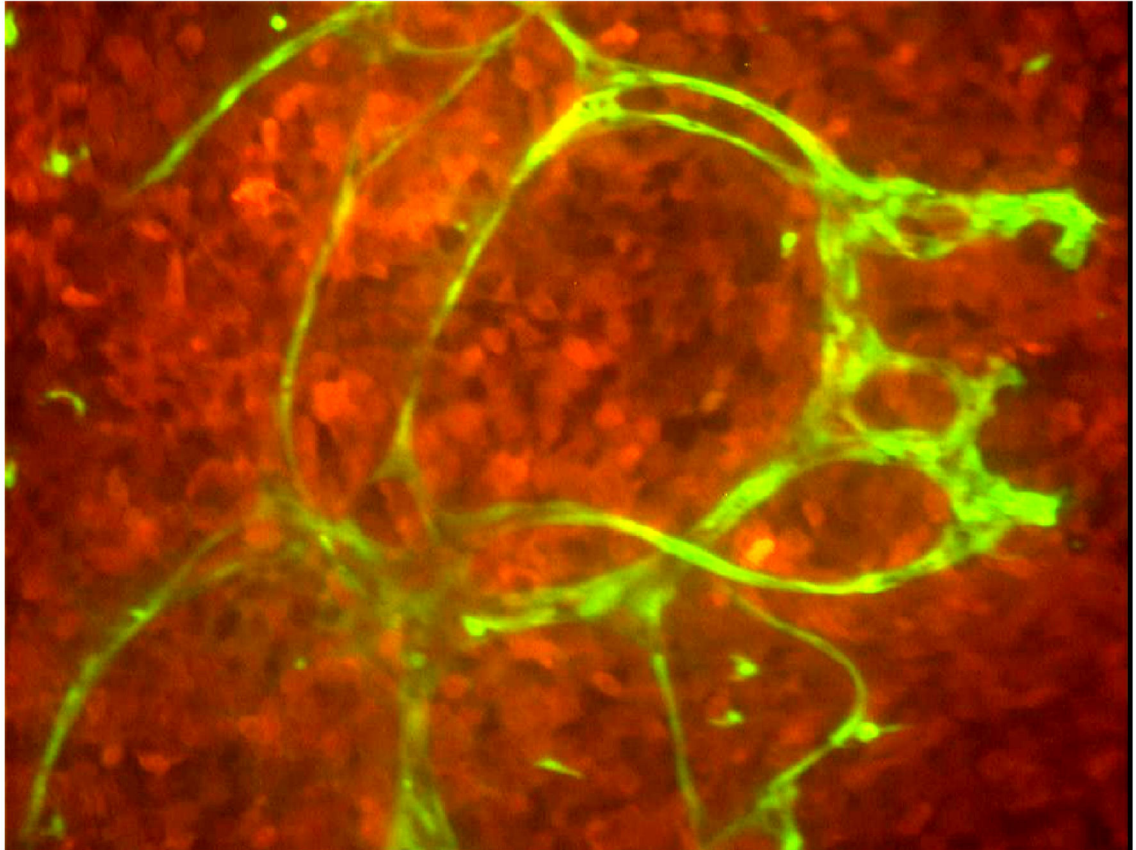


Figure 6. Visualization of angiogenesis in live tumor tissue 3 weeks after s.c. injection of B16F10-RFP melanoma cells in the transgenic GFP mouse
Well developed, host-derived GFP-expressing blood vessels are visualized in the RFP-expressing mouse melanoma.⁸¹

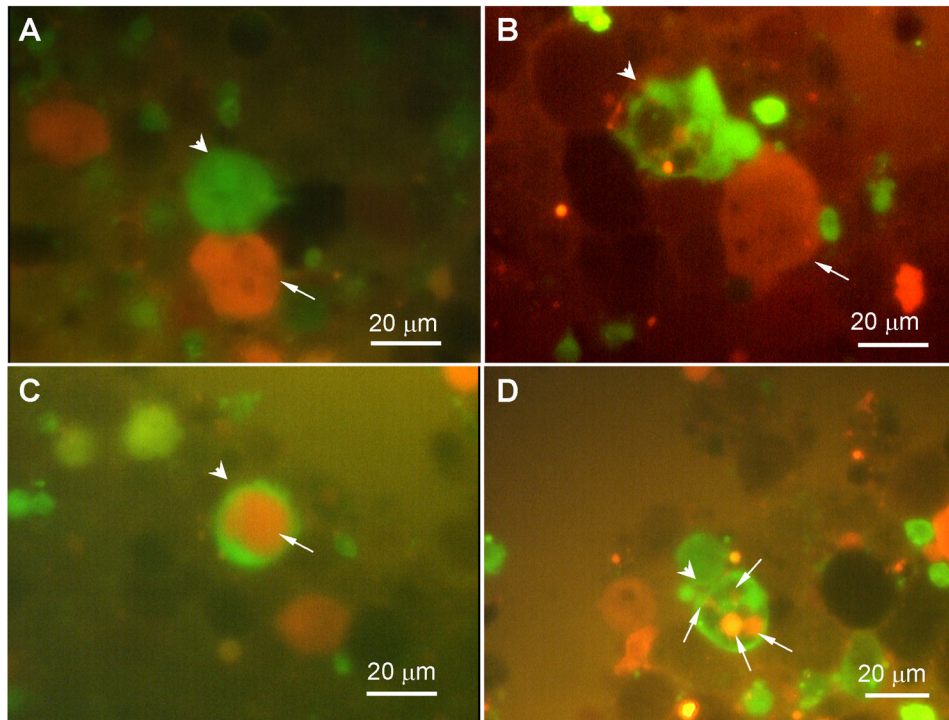


Figure 7. Visualization of host macrophage–tumor cell interaction in fresh tumor tissue
Images show host macrophages expressing GFP interacting with human PC-3-RFP prostate cancer cells on day 35 after orthotopic implantation of PC-3-RFP cells in the transgenic GFP nude mouse. **(A)** Host GFP macrophage (arrowhead) contacting RFP cancer cell (arrow). **(B)** GFP macrophage (arrowhead) engulfing RFP cancer cell (arrow). **(C)** RFP cancer cell (arrow) engulfed by GFP macrophage (arrowhead). **(D)** RFP cancer cell (arrows) digested by GFP macrophage (arrowhead). (Scale bars, 20 μm.)⁸¹

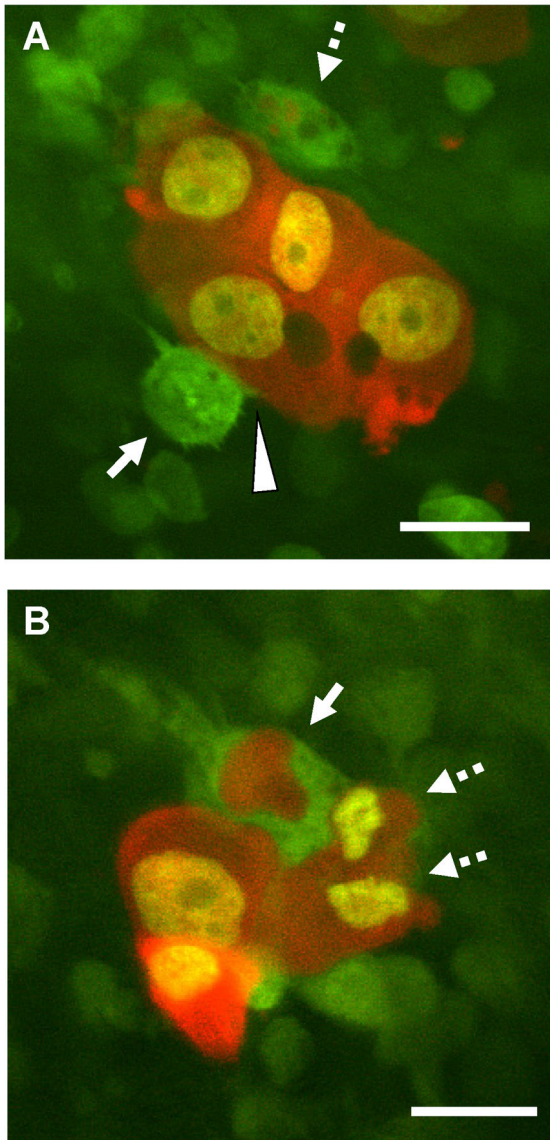


Figure 8. Visualization of host macrophage-cancer cell interaction in live mice

(A) Host GFP macrophages were visualized contacting HT-1080-GFP-RFP cells (arrow, broken arrow). Macrophage processes can be seen extending into the HT-1080-GFP-RFP cell (arrowhead). Another macrophage (broken arrow) contained cytoplasmic fragments after digesting an HT-1080-GFP-RFP cell. (B) A macrophage (arrow), engulfing the RFP-expressing cytoplasm of an HT-1080 cell shown in contact with additional HT-1080-GFP-RFP cells (broken arrows). Bar=20 μm .⁸²

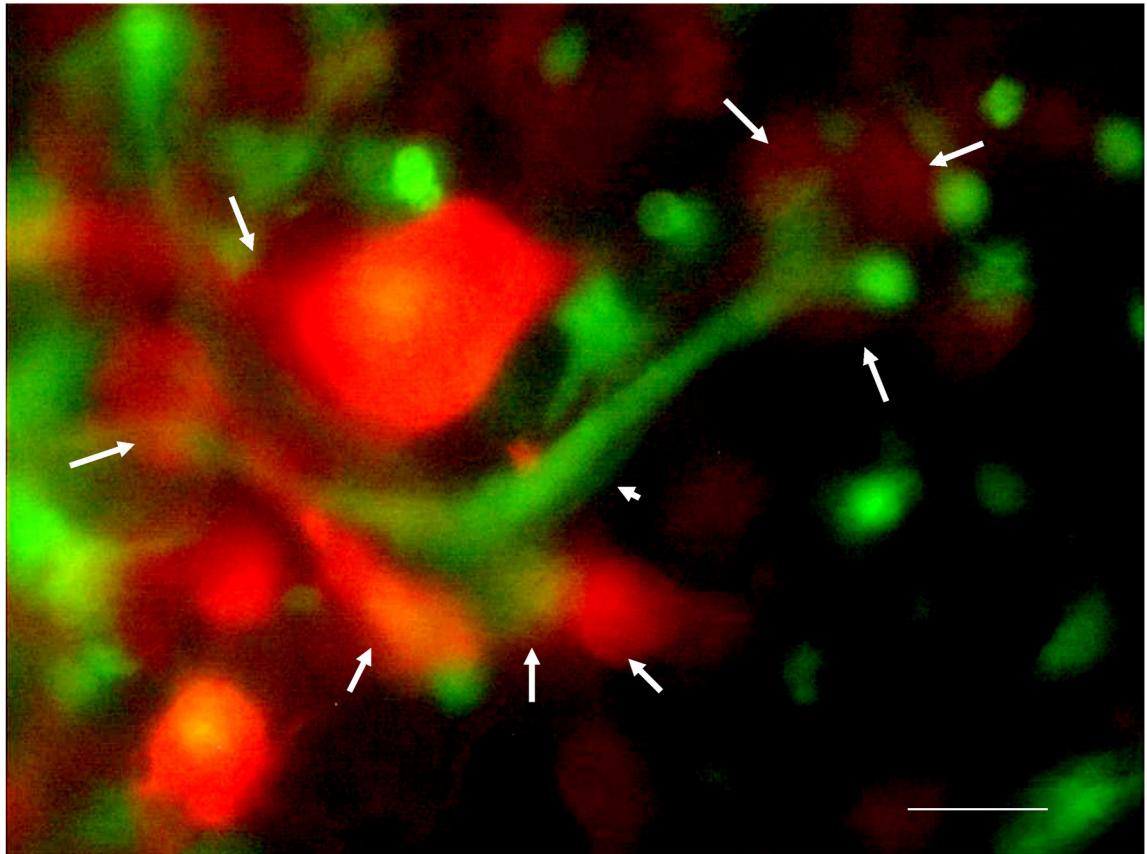


Figure 9. Interactions (arrows) of host stromal GFP-expressing fibroblast cell (arrowhead) and Dunning RFP-expressing rodent prostate cancer cells in live tumor tissue. Scale bar, 20 μm .¹¹⁶

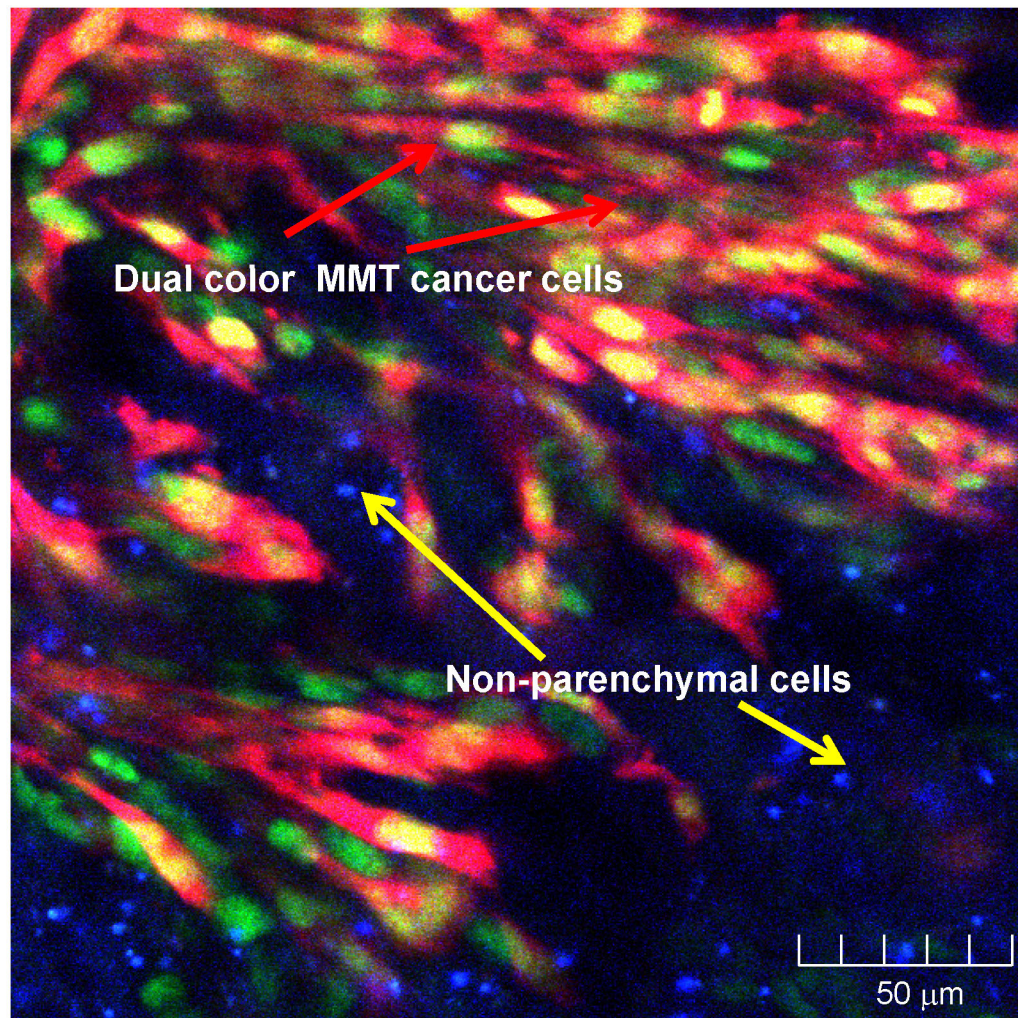


Figure 10. Dual-color MMT cells with GFP in the cytoplasm and RFP in the nucleus, growing in the liver of a CFP nude mouse after splenic injection

Dual-color MMT cells formed tumors in the liver of a CFP mouse 28 days after splenic injection. Hepatocytes, non-parenchymal liver cells (yellow arrows) and dual-color MMT cancer cells (red arrows) were visualized simultaneously. The image was taken with an FV1000 confocal microscope. (Bar=50 μm).⁸⁵

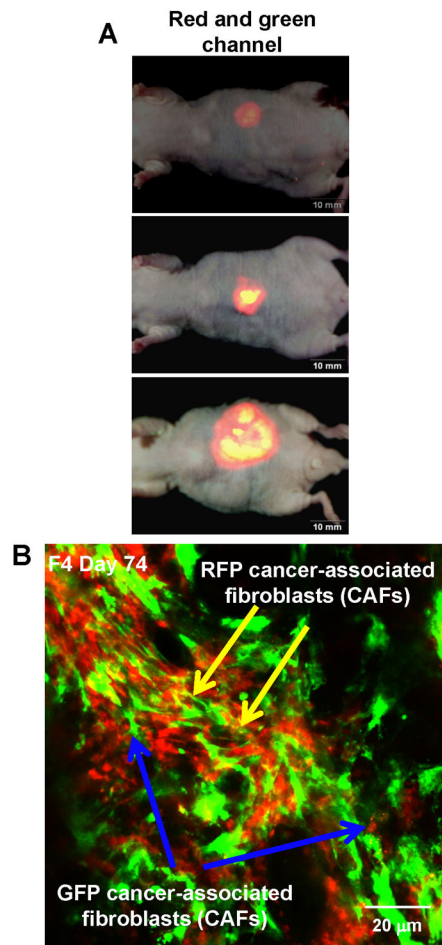


Figure 11. Non-invasive imaging of fluorescent tumor from a patient with pancreatic cancer growing orthotopically in nude mice

(A) Whole-body non-invasive imaging of human pancreatic cancer orthotopic tumorgraft in non-transgenic nude mice. Mice were non-invasively imaged at day-21 (upper panel), day-30 (middle panel) and day-74 (lower panel). The tumors in the non-transgenic nude mice are in the F4 passage after F1, in NOD/SCID mice after patient surgery; F2, in transgenic green fluorescent protein (GFP)-expressing nude mice; and F3 in transgenic red fluorescent protein (RFP)-expressing nude mice. The tumor acquired GFP and RFP stroma in the F2 and F3 passages, respectively. Images were taken with the Olympus OV100 Small Animal Imaging System. (B) Image of human pancreatic cancer tumor tissue resected from the F4 passage with RFP and GFP stroma. Image was taken with an FV1000 confocal laser microscope. Yellow arrows indicate RFP-expressing cancer-associated fibroblast cells (CAFs). Blue arrows indicate GFP-expressing CAFs.⁸⁹

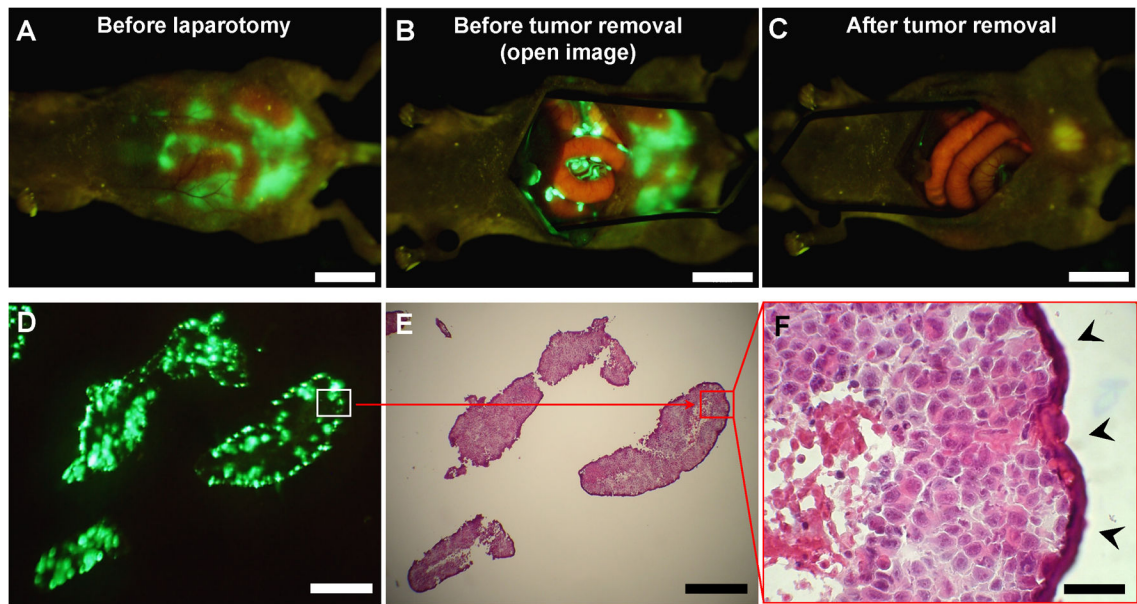


Figure 12. Fluorescence-guided surgical removal of peritoneal disseminated HCT-116 tumors after GFP labeling with OBP-401

Non-colored HCT-116 human colon cancer cells were injected into the abdominal space of nude mice. Ten days later, 1×10^8 PFU of OBP-401 were i.p. injected. (A) Disseminated nodules were efficiently labeled and noninvasively visualized by GFP expression 5 days after virus administration. (B) Under general anesthesia, laparotomy was performed to remove intra-abdominal disease under GFP-guided navigation. (C) Disseminated nodules visualized by GFP-guided navigation were removed. (Scale bars: A–C, 10 mm.) (D) Frozen section of resected HCT-116 disseminated nodules with fluorescence detection. (Scale bar, 500 μm .) (E) H&E section of HCT-116 disseminated nodules shown in D. The box outlines a region of D and E analyzed in F. (Scale bar, 500 μm .) (F) Detail of the boxed region of D and E. (Scale bar, 50 μm .)⁹⁶

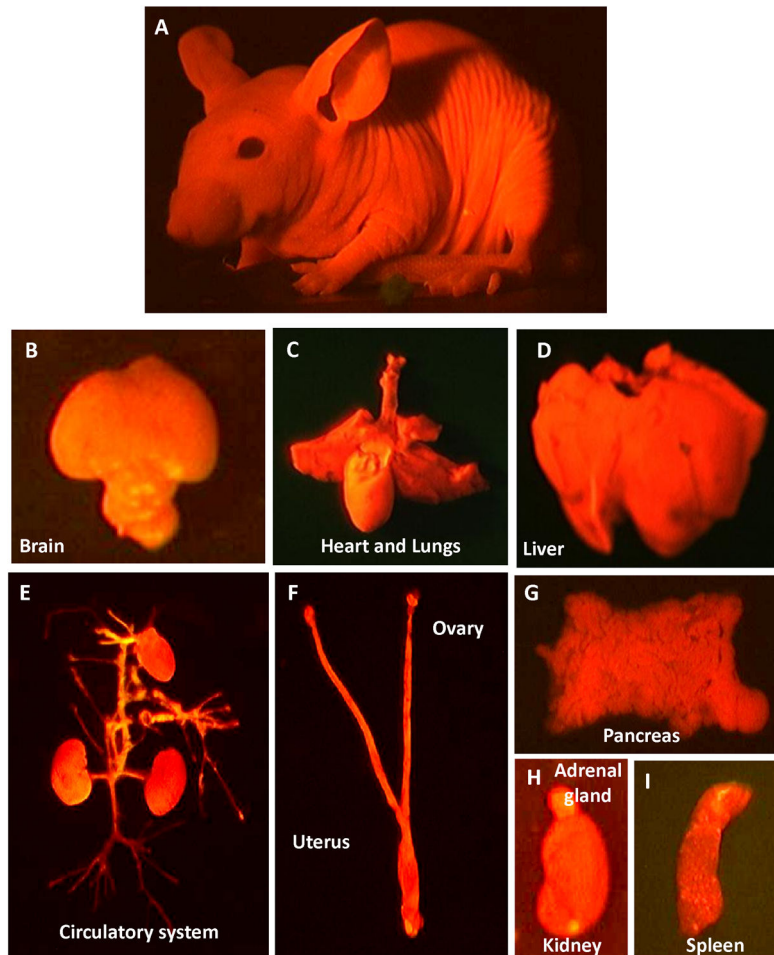


Figure 13. Transgenic RFP nude mouse

All of the major organs and tissues are red under fluorescence excitation with blue light. (A) Whole-body image of transgenic RFP nude mouse. Image was taken with a Hamamatsu C5810 tree-chip CCD camera. (B) Brain. (C) Heart and lungs. (D) Liver. (E) Circulatory system. (F) Uterus and ovary. (G) Pancreas. (H) Kidney and adrenal gland. (I) Spleen. (B-I) Images were taken with the Indec Biosystems FluorVivo imaging system.¹¹³

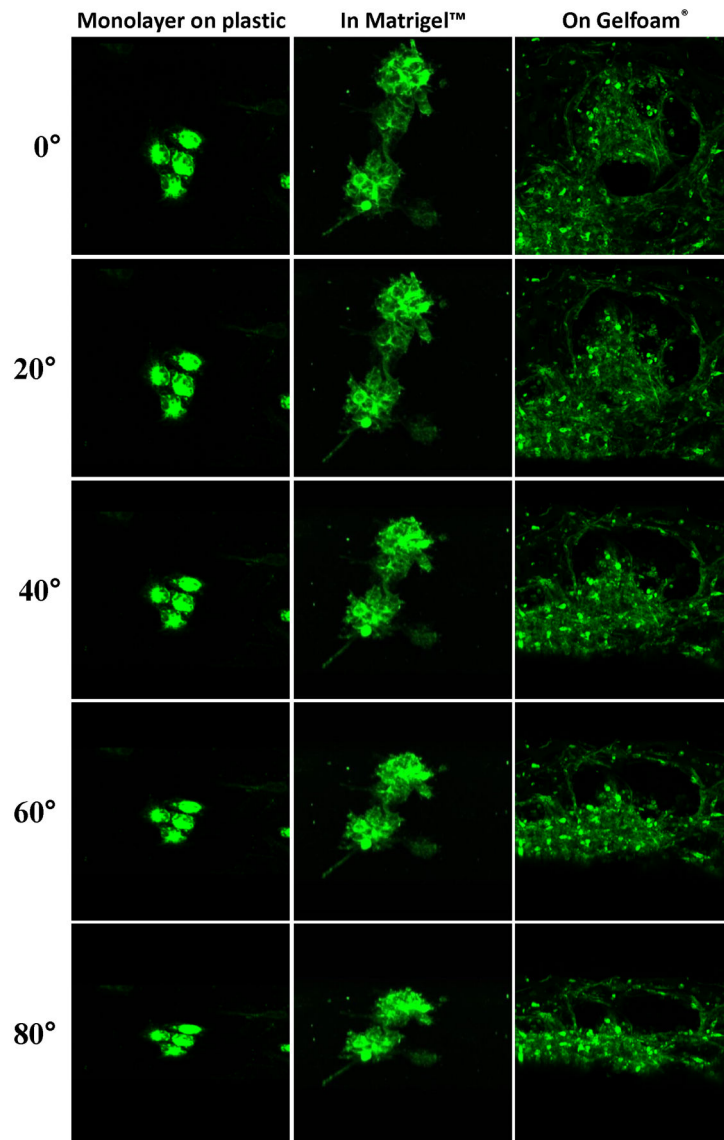


Figure 14.

Image rendering. Phase contrast fluorescence micrographs and rotating images of 143B human osteosarcoma cells expressing α_v integrin fused to GFP on plastic plates (left panels), in Matrigel™ culture (middle panels), in Gelfoam® culture (right panels) using the Olympus FV1000. Z-stack in 1 μm steps. The depths of images are on plastic surface 20 μm ; Matrigel™ 70 μm ; Gelfoam® 180 μm . These images are rotated around the Z axes from 0° to 80° in 5 sections, using the FV-10 ASW software system.¹¹⁵